

OPTIMIZATION OF T-SHAPED FULL ADDER USING PHOTONIC CRYSTAL

A thesis submitted by

SHIKHA SINGH

2017PWC5511

Under the guidance of

Dr. ASHISH KUMAR GHUNAWAT

In partial fulfilment for the award of the degree of

MASTER OF TECHNOLOGY

DEPARTMENT OF ELECTRONICS AND

COMMUNICATION ENGINEERING



Electronics & Communication Engineering Department

Malaviya National Institute of Technology, Jaipur

JUNE 2019



**DEPARTMENT OF ELECTRONICS & COMMUNICATION
ENGINEERING
MALAVIYA NATIONAL INSTITUTE OF TECHNOLOGY,
JAIPUR (RAJASTHAN) – 302017**

Certificate

This is to certify that the dissertation report entitled “**Optimization of T-Shaped Full Adder using Photonic Crystal**” submitted by **Shikha Singh** (2017PWC5511) in partial fulfilment of requirement for the award of the degree of **Master of Technology in Wireless & Optical Communication Engineering** submitted to Malaviya National Institute of Technology, Jaipur is a record of bonafide research work carried out by him under my supervision. The matter in the dissertation work in full or in part have not been submitted to any other university or institution for the award of any degree.

(Dr. Ashish Kumar Ghunawat)

Assistant Professor

Date :

Department of ECE

Place:

MNIT Jaipur, India



**DEPARTMENT OF ELECTRONICS & COMMUNICATION
ENGINEERING
MALAVIYA NATIONAL INSTITUTE OF TECHNOLOGY,
JAIPUR (RAJASTHAN) – 302017**

Declaration

I, **Shikha Singh**, declare that the dissertation report entitled “**Optimization of T-Shaped Full Adder using Photonic Crystal**”, being submitted by me in partial fulfilment of the degree of **M.Tech (Wireless and Optical Communication)** is the research work carried out by me under the supervision of **Dr. Ashish Kumar Ghunawat** and the content of this dissertation report, in full or in part, have not been submitted to any other university or institute for the award of any degree. I also certify that no part of this dissertation report has been copied or borrowed from anyone else. In case any type of plagiarism is found out, I will be solely and completely responsible for it.

Date:

Shikha Singh

Place:

2017PWC5511

Acknowledgement

I would like to thank all peoples who have helped me in this project, directly or indirectly. I am especially grateful to my supervisor Dr. Ashish Kumar Ghunawat (Assistant Professor, Dept. of ECE, MNIT Jaipur) for his invaluable guidance during my project work, encouragement to explore parallel paths and freedom to pursue my ideas. My association with him has been a great learning experience. He made it possible for me to discuss with a number of people and work in different areas.

I express my sincere gratitude to Dr. D. Boolchandani (Head of Department) for his support and guidance in this research work. Many thanks to committee members Dr. Ghanshyam Singh (Associate Professor), Dr. Vijay Janyani (Associate Professor), Dr. Ritu Sharma (Associate Professor) and Dr. M. Ravi Kumar (Assistant Professor) for their valuable comments and guidance in research exploration, without this guidance it was not possible to achieve these good results in this research work. I would like to thank Mr. Vijay Singh and Mr. Dipak for allowing me in laboratories over time. I am also very thankful to my friend Mr. Nilesh Kumar Yadav for their valuable suggestions and discussion, which I had with them about this research work. They also help me in designing work of my project.

I would also like to thank Ministry of HRD, Government of India for its support to me to pursue my Masters in Wireless and Optical Communication Engineering from Malaviya National Institute of Technology, Jaipur. This support provided me library, laboratory, hostel and other related infrastructure.

Shikha Singh

ABSTRACT

All-optical logic gates for the full adder structure have been implemented with focus on a 2-D PhC (photonic crystal) comprising of silicon (Si) air holes based square lattice. We have proposed in this work, a full adder structure based on PhC that makes use of 3 T-shaped waveguides focused on PhC. Three inputs and two outputs and an additional input that act as controlling input (D_i) have been used in the structure. Controlling input creates a phase between inputs produce outputs SUM and CARRY. The type of output logic acquired from the SUM and CARRY ports is calculated by the interference model based on path difference involved. That contrast ratio is 12.5 dB and 6.5dB respectively, it is ratio of power for minimum value of logic '1' to logic '0' for SUM and CARRY. 0.37ps is the evaluated fast response time of the implemented design. Furthermore, the required C-band procedure is continuous up to 1550 nm. The efficiency and design of the desired structure was verified using the Finite difference time domain (FDTD).

List of Abbreviations

1D	-	One Dimensional
2D	-	Two Dimensional
3D	-	Three dimensional
PhC	-	Photonic crystal
CR	-	Contrast ratio
PWE	-	Plane wave expansion
FDTD	-	Finite difference time domain
PBG	-	Photonic band gap
SC	-	Self-collimation
Si	-	Silicon
PML	-	Perfectly matched layer
CAD	-	Computer aided design
TIR	-	Total internal reflection
TE	-	Transverse electric
TM	-	Transverse magnetic
OFD	-	Optical field distribution
PCRR	-	Photonic crystal ring resonator
OPL	-	Optical power level
FA	-	Full adder

List of Symbols

μm	-	Micrometer
KHz	-	Kilo Hertz
THz	-	Tera Hertz
Tbps	-	Tera bits per second
dB	-	Decibel
Nm	-	Nanometer
a	-	Lattice constant
Λ	-	Wavelength
cT	-	micrometer
P_1	-	Power of logic '1'
P_0	-	Power of logic '0'
ps	-	Pico second
ρ	-	Equivalent magnetic loss
σ	-	Electric conductivity
ϵ_r	-	Relative permittivity
ϵ_0	-	Free space permittivity
μ_r	-	Relative permeability
μ_0	-	Free space permeability

CONTENTS

ABSTRACT	v
List of Abbreviations	vi
List of Symbols	vii
List of Figures	xi
List of Tables	xiii
CHAPTER 1	1
INTRODUCTION	1
1.1 Motivation	2
1.2 Objective of Thesis.....	2
1.3 Thesis organization	2
CHAPTER 2	4
Literature Survey	4
CHAPTER 3	8
PHOTONIC CRYSTAL	8
3.1 History of Photonic Crystal.....	8
3.2 Theory of Photonic Crystal	8
3.2.1 1D-PhC: One Dimensional Photonic Crystal	9
3.2.2 2D PhC: Two Dimensional Photonic crystal.....	10
3.2.3 3D – PhC: Three Dimensional Photonic Crystal.....	12
3.3 Types of Defects.....	13
3.3.1 Point Defects.....	13
3.3.2 Line Defects and Waveguide.....	13
3.4 Merits of Photonic Crystals.....	14
CHAPTER 4	15
SOFTWARE DESCRIPTION	15
4.1 RSoft Software	15
4.1.1 Basic 2D Simulation.....	15

4.1.2 CAD Window Basics	15
4.1.2 Creating a New Design File	16
4.1.4 Selecting Initial Settings:.....	16
4.1.5 The Layout Window:.....	17
4.1.7 Adding the Waveguide	19
4.1.8 Drawing the Waveguide:	19
4.1.9 Choosing the Excitation.....	19
4.1.10 Adding a Monitor	21
4.1.11 Performing the Simulation.....	22
4.1.12 The Simulation Window.....	23
4.1.13 Accessing Saved Data	23
4.1.14 Opening Plots	24
4.1.15 Viewing the Plotting Commands.....	24
4.1.16 Viewing the Raw Data.....	24
4.2 Operating Principle	24
4.2.1 Constructive Interference	24
4.2.1 Destructive Interference	25
4.3 Numerical Analysis	26
4.3.1 Maxwell's equations.....	26
4.3.2 PWE Method	26
4.3.3 FDTD Method	28
CHAPTER 5	30
DESIGN PROCEDURE AND OPTIMIZATION	30
5.1 Design Procedure	30
5.2 Analysis on the basis of optimization of edge rods re_1 , re_2 and re_3	32
CHAPTER 6	34
RESULT AND ANALYSIS	34
6.1 Optical Field Results	34
6.1.1 Simulation Results for $A = 0$, $B = 0$, and $C = 1$	34
6.1.2 Simulation Results for $A = 0$, $B = 1$, and $C = 0$	35

6.1.3 Simulation Results for $A = 0$, $B = 1$, and $C = 1$	35
6.1.4 Simulation Results for $A = 1$, $B = 0$, and $C = 0$	36
6.1.5 Simulation Results for $A = 1$, $B = 0$, and $C = 1$	36
6.1.6 Simulation Results for $A = 1$, $B = 1$, and $C = 0$	37
6.1.7 Simulation Results for $A = 1$, $B = 1$, and $C = 1$	38
6.2 Optical Power Levels Of Sum And Carry Outputs	40
6.2.1 $A = 0$, $B = 0$ and $C = 1$	40
6.2.2 $A = 0$, $B = 1$ and $C = 0$	41
6.2.3 $A = 0$, $B = 1$ and $C = 1$	41
6.2.4 $A = 1$, $B = 0$ and $C = 0$	42
6.2.5 $A = 1$, $B = 0$ and $C = 1$	42
6.2.6 $A = 1$, $B = 1$ and $C = 0$	43
6.2.7 $A = 1$, $B = 1$ and $C = 1$	43
6.3 Response Time Calculation.....	44
CHAPTER 7	47
CONCLUSION AND FUTURE SCOPE.....	47
7.1 Conclusions	47
7.2 Future scope	47
REFERENCES	48

List of Figures

Figure 3.1: 1D-PC cross-section constant of two layers of the similar width ($0.5a$) and distinct dielectric constants. A is a period of lattice. Dielectric constant periodically differs in the direction of z and is uniform in the plane of x - y	9
Figure 3.2: Band diagram of 1D-PhC in which intervals of dielectric layers of similar width ($0.5a$) have (a) similar dielectric constants, (b) minute distinction in dielectric constants (c) more distinction in dielectric constants.....	10
Figure 3.3: Cross-section of 2D-PhCs including of square lattice (a) lengthy circular holes of the dielectric constant in the air background; (B) circular air rods in the dielectric constant slab.....	11
Figure 3.4: First Brillouin Zone (BZ) square 2D-PhC lattice.....	11
Figure 3.5: (a) displays a 2D-PhC square lattice band diagram composed of long dielectric circular holes of the dielectric constant in the air background. A period of lattice (b) appears the same structure band diagram for TE modes TM modes	11
Figure 3.6: (a) 3D-PhC schematic: woodpile design [28] created by stack of dielectric rectangular holes of dielectric constant 12.96 with alternating orthogonal orientations in the background of air. (b) Shows band diagram of above structure.....	12
Figure 3.7: (a) Displays the 2D-PhC cross-section with a point defect. Inside the standard crystal, a point defect was formed by removing the central hole. Super-cell was labeled with a black dashed square with 6 x - and z -points. (b) Shows TM mode, Localized frequency.	13
Figure 3.8: (a) demonstrates the 2D-PhC cross-section with a number of point defects. Within the periodic crystal, series of point defects were developed by removing the core column rods. Super-cell was labeled with a black dashed rectangle with x -direction lattice	14
Figure 4.1: The RSoft CAD layout window, appearing the menu bar at the top, the top and left toolbars, and the status line at the bottom	15
Figure 4.2: The startup dialog that appears whenever a new design file is created.....	16
Figure 4.3: CAD Layout	18
Figure 4.4: Symbol Table Editor: its variable Length with such a value of 10 was described.....	18
Figure 4.5: The straight segment since drawing because it appears. It shows a domain of simulation and also the field of launch.....	19
Figure 4.6: Its segment characteristics dialog in the above model for the segment. Of this example, they will set the waveguide's length is $10\ \mu\text{m}$	19
Figure 4.7: The Launch Parameters dialog.	20

Figure 4.8: The FullWAVE Simulation Parameters dialog where the Default Launch settings are located.....	21
Figure 4.9: The properties dialog for a monitor.....	21
Figure 4.10: The completed structure in the CAD with the monitor created.	22
Figure 4.11: A distinct program in simulation after waveguide structure has been simulated. A graphic display demonstrates the optical field's color-coded contour plot.....	23
Figure 4.12: The WinPLOT window that demonstrates this simulation's monitor outcome.	23
Figure 4.13: Viewing the Plotting Command.....	24
Figure 4.14: Constructive Interference	25
Figure 4.15: Destructive Interference	25
Figure 5.1: Combinational circuit diagram of Full Adder	31
Figure 5.2: Lattice structure for Full Adder.....	31
Figure 5.3: Band diagram for FA structure.....	32
Figure 6.1: OFD for chosen i/p combinations $A=0$, $B=0$, and $C=1$	34
Figure 6.2: OFD for i/p combinations $A=0$, $B=1$, and $C=0$	35
Figure 6.3: OFD for i/p combinations $A=0$, $B=1$, and $C=1$	36
Figure 6.4: OFD for i/p combinations $A=1$, $B=0$, and $C=0$	37
Figure 6.5: OFD for i/p combinations $A=1$, $B=0$, $C=1$	37
Figure 6.6: OFD for i/p combinations $A=1$, $B=1$, $C=0$	38
Figure 6.7: OFD for i/p combinations $A=1$, $B=1$, $C=1$	39
Figure 6.8: OPL at the ports SUM and CARRY for the input combinations $A=0$, $B=0$, and $C=1$ (blue – SUM, green - CARRY)	40
Figure 6.9: OPL at the ports SUM and CARRY for the input combinations $A=0$, $B=1$, and $C=0$ (blue – SUM, green - CARRY)	41
Figure 6.10: OPL at the ports SUM and CARRY for the input combinations $A=0$, $B=1$, and $C=1$ (blue – SUM, green – CARRY).....	41
Figure 6.11: OPL at the ports SUM and CARRY for the input combinations $A=1$, $B=0$, and $C=0$ (blue – SUM, green – CARRY).....	42
Figure 6.12: OPL at the ports SUM and CARRY for the input combinations $A=1$, $B=0$, and $C=1$ (blue – SUM, green – CARRY).....	42
Figure 6.13: OPL at the ports SUM and CARRY for the input combinations $A=1$	43
Figure 6.14: OPL at the ports SUM and CARRY for the input combinations $A=1$, $B=1$, and $C=1$ (blue – SUM, green – CARRY).....	43
Figure 6.15: Time evolving curve from port SUM.....	45
Figure 6.16: Time evolving curve from port CARRY.....	46

List of Tables

TABLE 4.1: CHOOSING INITIAL STAGE.....	17
TABLE 5.1: TRUTH TABLE FOR FA.....	32
TABLE 6.1: PROPOSED FULL ADDER: SUMMARY OF CR.....	39

CHAPTER 1

INTRODUCTION

The semiconductor has since played a major role in our everyday life and distantly revised the earth. However, the technical reports and the high speed of the electrical circuit were also carried out worldwide currently. This minimization of the circuit results in increased resistance and increased power failures. To attain the high speed of technological and durable circuits, the researchers switched to photon rather than electrons. There are several pros and cons to light over electrons. The optical system bandwidth is in THz order, but the electronic system's bandwidth is just kHz [16, 17]. Since the information carries are photons, they are not communicating with environmental disruption. Although the effectiveness of electronic systems is improved with each day, a new optical material referred as photonic crystal is introduced. The main idea behind PhC design is the material requirement that controls photon flow.

The conventional method used to regulate photon flow is the total internal reflection. Furthermore, the photonic crystals provide a better system of light security. Photonic bandgap controls the flow of light. Several advantages include compactness, containment, and low cost. By designing the photonic band such as optical fiber, resonator, logic gates, among others. There are many applications. In order to gain the full benefit of all optical digital technologies, all communication measures must be carried out in the optical domain without using any electronics. Full adder (FA) seems to be a combination circuit where three binary bits can be added, resulting in two outputs, one being SUM, a next is CARRY.

Achieving complete benefits of all-optical communication technologies needs all communication measures to be performed in either the optical domain with no electronics being used. For optical systems, signal processing however is very essential. To send out the all-optical signal processing, they involve all-optical logic systems. But, with an all-optical FA, since all four basic mathematical operations including addition, subtraction, multiplication, and division can be done using optical FA [6], it is an essential instrument for the application of optical signal processing. However, FDTD is a vital tool for applying optical signal processing. Implemented structure for all-optical logic gates in 2-D PhC waveguides centered on optical

interference impact. In this project introduced 3 input ports and on controlling input port. This controlling input port creates phase difference between input ports and controlling input and produced constructive or destructive interference [2].

1.1 Motivation

Photonics technology has multiple benefits over semiconductor technology.

- a) Due to faster signal transmission, photons in such a dielectric medium may propagate faster than electrons in either a metallic medium.
- b) Photons interact less frequently than electrons resulting in less energy loss.
- c) Photons can carry more data than electrons, which leads to construction for high density.

PhC's are regarded as artificial crystal structures that prohibit the propagation of light wave of a particular frequency range. This range of prohibited frequencies is often named as PBG (the Photonic Band Gap). Because of their ability to regulate and manipulate light, these buildings have been recognized as prospective applicants for compress all-optical communication and manipulating systems. To PhC-based systems, extreme miniaturization and quite low workings power are feasible. On other hand, the dispersion features of bulk PhC's were intended to prevent divergence of light beams in particular directions.

This is called self-collimation (SC) phenomenon. In total PhC's, the focused on SC affect, interferometers, splitters and bends, resonators, combiners, switches etc.

1.2 Objective of Thesis

Optimization of T-Shaped Full Adder using Photonic crystal project has been proposed using FDTD with PML using RSoft full wave software. To improve contrast ratio by optimizing the power of output port for logic 0 and 1. Contrast ratio can be called as the ratio of response power when the output logic is high to the power when the output logic is low. To increase contrast ratio by optimizing corner holes in T-Shaped.

1.3 Thesis organization

Introduction, motivation and objective of thesis are presented in Chapter 1. Chapter 2 discusses the state of art, where an extensive analysis on literature is presented. The first step is to study the associated documents earlier released by researchers in order

to start with the thesis. Reviewing the literature helps make this job easy. Chapter 3 involves the history of PhC and introduction of PhC. In chapter 4 presents numerical techniques (i) PWE and (ii) FDTD. These techniques were used to investigate the propagation of light and to model suggested structures, operating principle and about the software used. Chapter 5 deals with the design of the Full Adder with focus on 2D PhC that comprises of square lattice of air holes on silicon. The implemented structure has been simulated using the FDTD technique and the results shows that any logical operation can be implemented through the introduction of an appropriate original stage between the input beams in order to interfere either constructively or destructively based on the application of interest. Further, it involves an optimization of the Rods re_1 , re_2 and re_3 for structure analysis. Chapter 6 discuss the simulation and outputs the results followed by chapter 7 that concludes the work and gives the future scope.

CHAPTER 2

Literature Survey

In latest years, as shown in this chapter, the optical logic gate based on PhC has received much interest. Many scientists have now begun to pay more attention to designing photonic crystal optical logic doors, as it is one of the most significant optical media to shape optical processors, information handlers, and optical communication systems. As shown in this section, optical logic gates are usually split into three design and manufacturing classifications such as resonators, interference waveguide, and self-collimation. Some writers have intended the resonator-based logic gate. These can be linear or nonlinear resonators. Some of the writers used the interference waveguides to study the optical gate. The literature study of all Photonic Crystals-based optical logic gates by multiple scientists over the previous few years is shown below:

Yin - Pin Yang et al. [1]

The writers showed a structure of all the optical gates AND gate in triangular lattice based on 2-D PhC. It has two port of input and one port of output. It consisted of a sandwiched PCRR waveguide between two waveguides input. The device's electrical field distribution is evaluated using the FDTD technique. Due to total internal reflection (TIR) and resonator interference, the optical logic AND gate can operate at distinct wavelengths in the communication window of 1.3 μm and 1.55 μm . The definition of high ' 1 ' and low ' 0 ' logic levels is regarded to be more than 95% and less than 35% respectively. In multi-wavelength optical logic circuits, this design discovers the applications.

Preeti Rani et al. [2]

The author provided a structure of all the optical AND gate focused on Si substrate 2D (Two dimensional) triangular lattice photonic air holes crystal .It consisted of a linear waveguide in Y-shaped form without any individual instruments such as optical amplifiers. The system is evaluated and simulated using the respective PWE and FDTD methods. She explained the technique of discovering the working parameters.

Where elevated contrast ratio is acquired, the optimized parameters are determined. Optical logic gate power consumption is small because it is based on linear material. The device's contrast ratio is high to low logic power ratio. For this framework, it is only 6dB. In the realization of devices and elements for optical communication scheme and networks, this design discovers its application. This design is beneficial for implementation on a big scale and can be used in integrated circuits on chip photonics.

Preeti Rani et al. [3]

The author proposed in this paper designing all-optical gates that use the universal NAND gates arrangement. The PhC design consists of the lattice configuration of triangular silicon air holes. Intended and optimized an all-optical NAND gate. Also, the optimized NAND gates were used and arranged in combination to ensure the NOT, AND, OR, XOR and XNOR as an all-optical gate is specifically the combined structure. The truth table has been confirmed for the built all-optical logic gates for an operating wavelength of 1.55 nm. The indicated all optical gates indicate a response time of 2.168 ps with a 0.461 Tb / sec bit rate. Moreover, for the submitted doors, the CR has also been obtained. Achievement of the presented PhC framework was assessed using the PWE technique and the optimization characteristics were designed by FDTD.

Enaul Haq Shaik et al. [4]

The author designed a half adder PhC by the use of T-shaped waveguides no use of non-linear material Kerr type. One is an AND gate and the other being controls the output of AND gate that produce the SUM and CARRY. The third input creates a phase between inputs by interference principle. The fast response to the half adder is 0.48ps by the sum and carry. CR is known as the power ratio to logic 1 to logic 0. CR for sum and carry are the 5.17dB. The desired structure performs the C-band that's limit up to 1550 nm in continuously in nature. It can be used in its implementation of linked PhC because the region is very small.

Enaul Haq Shaik et al. [5]

The author proposed Half adder focused on all-optical PhC is presented taking T-shaped waveguides in 180° phase shift with inputs. T-shaped waveguides as light beam splitters throughout the input segment that will provide input to only the T-shaped waveguides well into the output segment that acts as energy combiners varying on both the transition stage. Carry is the output that creates 180° phase shift and to produce inputs. The simulated results produced CR is 10.95dB and 4.32dB for the sum and carry respectively and produced 1 Tbps bit rate.

Hamed Alipour-Banaei et al. [6]

The author implemented a structure for a 1-bit full adder focused on PC. This structure designed by the cascading of two half adders. Having eight waveguides and dual nonlinear rings in this structure and generated inside rod 2-D PC with square lattice. In this structure, a design has "A," "B" and "C" inputs and "SUM" and "CARRY" output ports. Its FDTD has verified the effectiveness and interface of the indicated structure work. Through adding two 1-bit optical half-adders, the author suggested an all-optical 1-bit FA focused on PhC ring resonators.

Chunrong Tang et al. [7]

In this paper, authors designed various all optical logical gates on a 2-D Photonic crystal. These design of logic gate based on multimode interference (MMI). It has two input port structure. The phase shift is introduced by different length of input waveguides. By introducing the phase shift, these logic gates are directly used for BPSK signals. The various logic gates which realized are OR, NAND, XNOR and XOR. The structures are analyzed and simulated using FDTD and PWE method. Two types of logic gates (XNOR/XOR) are designed: without bend and with bend. The contrast ratio for logic OR and NAND gates is 13dB, for XNOR is 17dB and for XOR is 21dB in the C-Band (1530– 1565nm). Since nonlinear material is not used so power consumption is less and the size of component is small. Hence the layout of logic gate has the potential to constitute PICs that will be utilized in all optical signal processing, all optical networks and photonic computing.

Yuan Fu et al. [8]

In this paper, the author theoretically designed five kinds of all optical logic gates in a 2-D single photonic crystal lattice simultaneously. The five kinds of optical logic gates are NOT, OR, NAND, XOR and XNOR gates. This structure based on the interference effect of light beam. This ingenious design consists of waveguide. By controlling the optical path difference, the different gates are possible to realize. These gates do not required high power for their logic function. The maximum contrast ratio is 20dB. This offers an effective and a simple attain for the design of integrated all-optical logic devices.

Yu-Chi Jiang et al. [9]

The authors realized the five different types of logic functions based on 2D PhC waveguide structures. The five different logic gates are NOT, OR, NOR, XNOR and +B. These gates are realized by choosing different reference and input ports. It based on the theory of interference of light beam. These gates are analyzed and simulated by the FDTD method. The logic level high and low is defined as the transmittance ratio larger than 0.5 and less than 0.1 at the output port, respectively. This investigation is carried out without considering phase difference between input beams. By considering the phase differences, the electric field distribution is altered. For this case high transmittance of 0.9 can be obtained. Therefore, the structure is favorable in optical device integration and also in the applications of waveguide in optical communications.

Susan Christina Xavier et al. [10]

In this paper, the authors presented an approach to plot all optical logic gate based on 2D PhC. This approach focused on the self-collimation effect in which beam spilt by line defect and interferes with the another self-collimated beams. That interference may be either destructive or constructive depends on the phase difference. The structure are analyzed by FDTD method to verify the functioning of design as logic gate AND, NAND, NOR and XNOR. The dimension of structure is $10\ \mu\text{m} \times 10\ \mu\text{m}$ only which results in high speed of operation. The contrast ratio of logic high to low is 6dB.

CHAPTER 3

PHOTONIC CRYSTAL

3.1 History of Photonic Crystal

Lord Rayleigh researched the photonic 1-D crystals in 1887, consisting of multi-layer dielectric stacks [11]. This research demonstrated the stop band defined as the the gap in the photonic band. The spontaneous emission, how it gets effected by band gap involved within the structure was investigated by Vladimir P. Bako [12]. He also gave 2-D and 3-D PhC structures theoretical concept [13]. Ohtaka created a formal band gap calculation for 3-D PhC constructions in 1979 [14]. In 1987, Yablonovitch and John released the two milestone documents. Yablonovitch's paper's primary concept was to regulate spontaneous emissions by engineering state density [15]. The concept of John's article was to use photonic crystal to regulate the flow of light [16]. The structure is hard to design on an optical scale. It results in most jobs that have been researched theoretically. In 1991, Yablonovitch introduced the first microwave system 3-D band gap [18]. Thomas Krauss showed the optical wavelength of the 2D photonic crystal in 1996 [19]. A number of study works has taken place around the globe to enhance optical processing and to use the PhC slab. Philip Russell established photonic crystal fiber for the first time in commercial use in 1998 [20]. Due to the level of building complexity, the research of 2-D photonic crystal is quick compared to 3-D. For better comprehension, there is study of naturally occurring PhC-based structure [21].

3.2 Theory of Photonic Crystal

PhC's take complete benefit of lights constant nature and hence open up a special area for growth and development of embedded devices for all sorts of optical applications. PhC's are simply ordered nanostructures where 2 different media with varying refractive indices or dielectric constants are used [22]. A high variation in the refractive index or dielectric constant may lead to minimal light absorption along with maximal reflections and refractions involved. This high rate of reflections and refractions at the interface can lead to many phenomenons that arises same as when electrons are considered by the periodical Coulomb potential [23].

As a result, periodic variations to dielectric refractive indices result in light-wave bands or band gaps [24]. PhC's could be categorized into other categories depending on a periodicity of that same variation throughout the dielectric refractive index:

3.2.1 1D-PhC: One Dimensional Photonic Crystal

The simplest PhC pattern comprises of multilayered design, a stack of materials/layers with varying dielectric constants. The stack is arranged in such a manner that there exist the dielectric constant variations only in a fixed single direction. The simple PhC stack also known as 1D-PhC is shown in Figure 1.1. In 1887 Lord Rayleigh demonstrated through his work, similar 1D-PhC's that may be used as Bragg mirror for the specific frequencies of light wave.

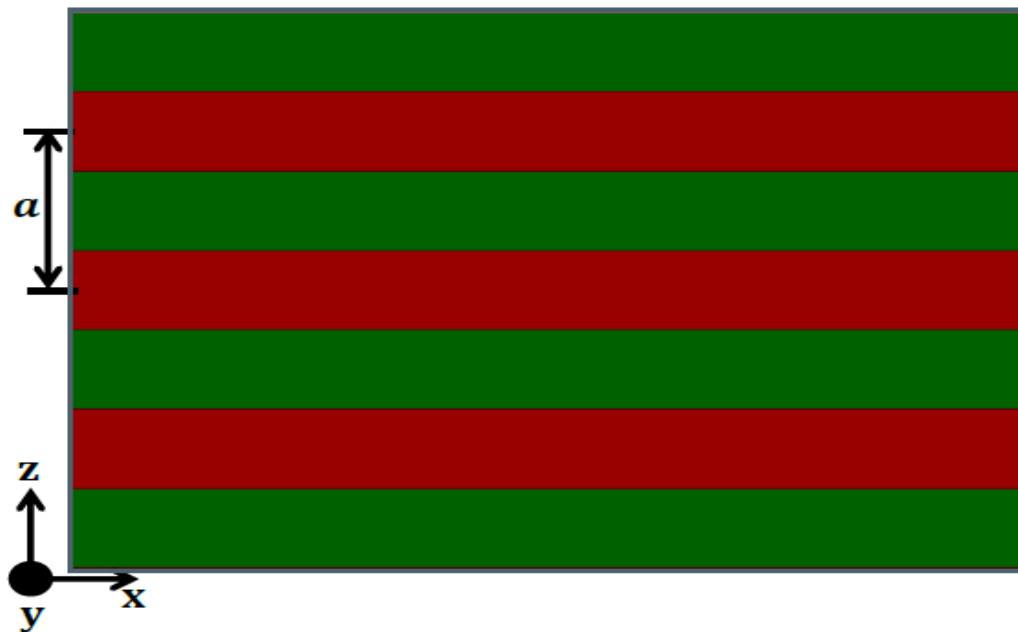


Figure3.1: 1D-PC cross-section constant of two layers of the similar width ($0.5a$) and distinct dielectric constants. A is a period of lattice. Dielectric constant periodically differs in the direction of z and is uniform in the plane of x - y .

All three case band / dispersion diagrams are shown in Figure 1.2 The technique acquired by PWE. This technique offers alternatives in periodic medium for Maxwell's equations. Maxwell's equations are discussed as detail in the next section in the regular medium and PWE technique.

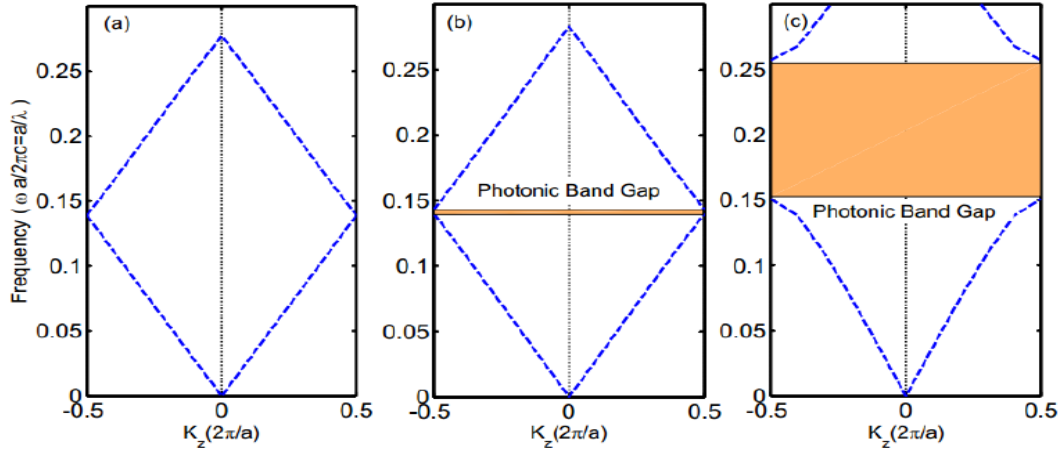


Figure 3.2: Band diagram of 1D-PhC in which intervals of dielectric layers of similar width ($0.5a$) have (a) similar dielectric constants, (b) minute distinction in dielectric constants (c) more distinction in dielectric constants

It's evident by figure 1.2(a) where intervals of layers have the similar dielectric constants, the whole medium becomes homogeneous in three directions and there is no gap at the edge of (BZ). In the picture 1.2(b), due to the slight difference in dielectric constants, a small gap between the upper and lower lines can be observed at the edge of Brillouin Zone BZ. This gap means that if the frequency falls within the gap, called PBG, no mode will be permitted to propagate through the framework. Next Fig 1.2(c) displays a broad PBG at the bottom of BZ owing to a greater distinction in the dielectric constants of the intervals of layers.

3.2.2 2D PhC: Two Dimensional Photonic crystal

2D-PhCs are categorized as structures with dielectric constant variation in two transverse directions and dielectric constant fixed in one direction. PBG may occur in the periodicity plane for 2D-PhCs.

Cases of 2D-PhCs are elevated dielectric constant columns integrated into low dielectric constant material and holes inserted in a strong dielectric constant slab. Figure shows a cross-sectional perspective of these constructions 1.3(a) and 1.3(b) in each case. Square lattice or triangular lattice can be used to arrange rods / holes. The systems presented in this thesis are focused on 2D-PhC square lattice containing rods, thus further off discussing the 2D-PhC square lattice involving rods.

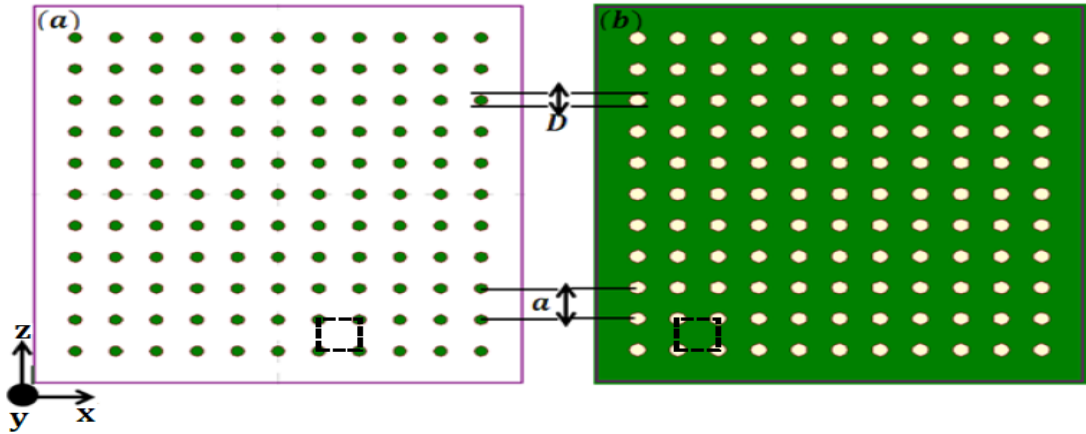


Figure 3.3: Cross-section of 2D-PhCs including of square lattice (a) lengthly circular holes of the dielectric constant in the air background; (B) circular air rods in the dielectric constant slab.

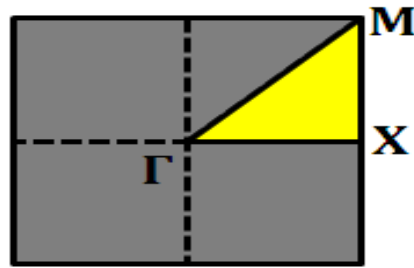


Figure 3.4: First Brillouin Zone (BZ) square 2D-PhC lattice.

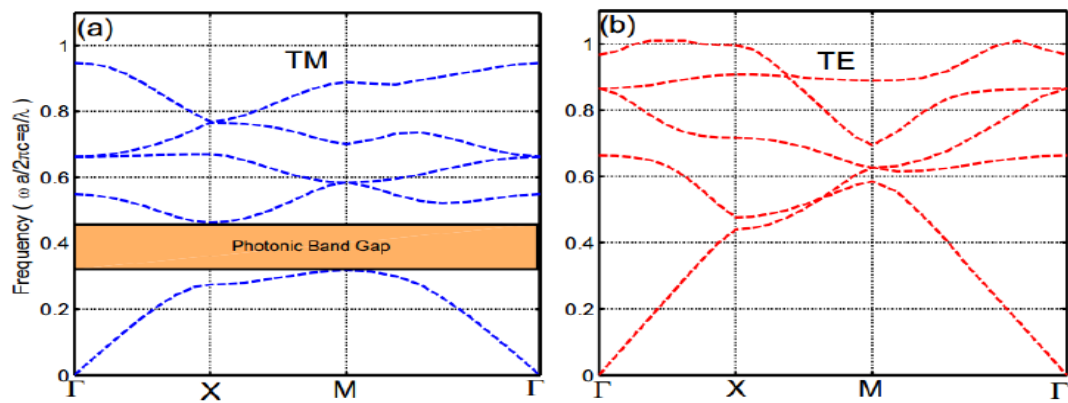


Figure 3.5: (a) displays a 2D-PhC square lattice band diagram composed of long dielectric circular holes of the dielectric constant in the air background. A period of lattice (b) appears the same structure band diagram for TE modes TM modes

The irreducible BZ indicates the yellow triangle Band diagram for TM and TE modes have been reached with PWE method and seen in Figure 1.5(a) and 1.5(b)

respectively. From Fig it's evident. 1.5(a) and 1.5(b) TM and TE band diagrams are completely distinct for the same structure. Indicate a PBG for standardized frequencies between 0.317 and 0.416 here TE modes have no PBG.

For standardized frequencies varying from 0.317 to 0.461, a PBG displays for TM modes (Fig. 1.5(a)), while no PBG becomes appear for TE modes (Fig. 1.5(b)). It is also possible to overlap PBGs of TM and TE modes, leading to a complete bandgap both for modes.

3.2.3 3D – PhC: Three Dimensional Photonic Crystal

Dielectric constant variable structures were classified as 3D-PhCs in three directions to provide complete light processing from all three directions. Wave vectors are discretized from all three directions for 3D-PhCs. This is possible to create 3D-PhCs with such a range of tubes/spheres that can be constructed in the type of cubes [25], face-centered cubes [18, 26] but also diamond lattices [26] face centered cubic [18, 26] and diamond lattices [26] .Yablonovitch first suggested PBG in all three directions in 1987.

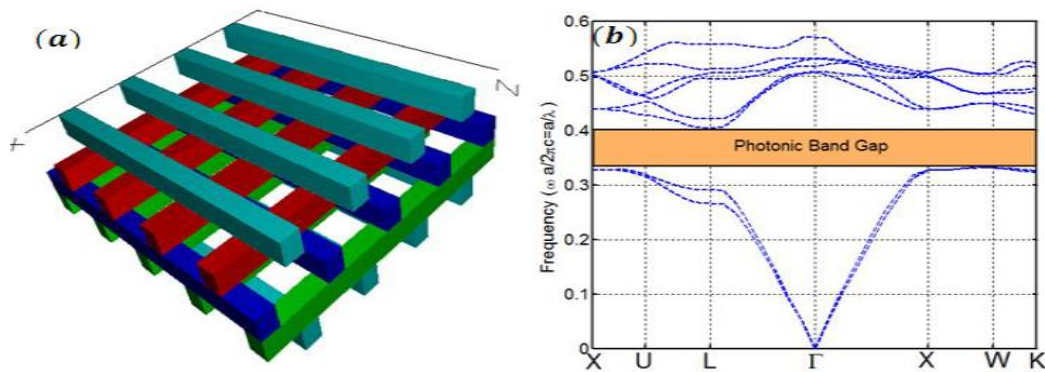


Figure 3.6: (a) 3D-PhC schematic: woodpile design [28] created by stack of dielectric rectangular holes of dielectric constant 12.96 with alternating orthogonal orientations in the background of air. (b) Shows band diagram of above structure.

Several designs have been produced to have 3D-PBG from then. Famous 3D-PhC kinds are woodpile [27], opal [28], and 2D-PhC stack [28]. For example, Figure 1.6(a) appears a 3D-PhC: woodpile design [27] created by a stack of dielectric rectangular holes of dielectric constant 12.96 with alternating orthogonal orientations in the

background of air. Band structure that matches Fig. 1.6(a) PWE technique acquired is seen in Figure. 1.6(b) [29] describes 3D-PhCs in detail.

3.3 Types of Defects

3.3.1 Point Defects

Point defect can be developed inside 2D-PhCs by removing a single rod or by increasing / decreasing the single rod radius. Within a point defect, one located mode or a set of tightly spaced modes may be developed. Localized point defect-supported modes cannot propagate throughout the remainder to the framework as their frequencies fall into PBG. These methods would also disappear from the defect exponentially.

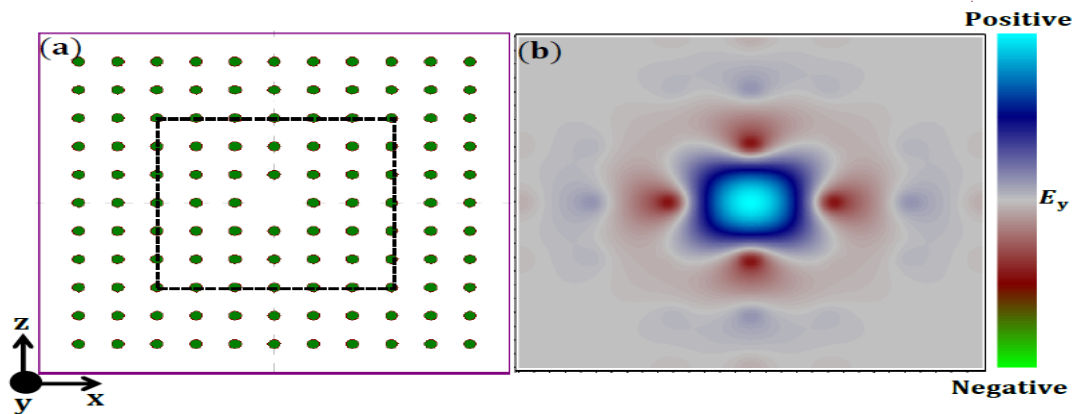


Figure 3.7: (a) Displays the 2D-PhC cross-section with a point defect. Inside the standard crystal, a point defect was formed by removing the central hole. Super-cell was labeled with a black dashed square with 6 x- and z-points. (b) Shows TM mode, Localized frequency.

3.3.2 Line Defects and Waveguide

It can be appears that within a periodic PhC structure a single point defect acts as a cage for light waves with frequencies within the PBG. That fundamental concept could be further expanded by sequentially disturbing holes of a single layer (either horizontal or vertical) to generate a waveguide for light waves.

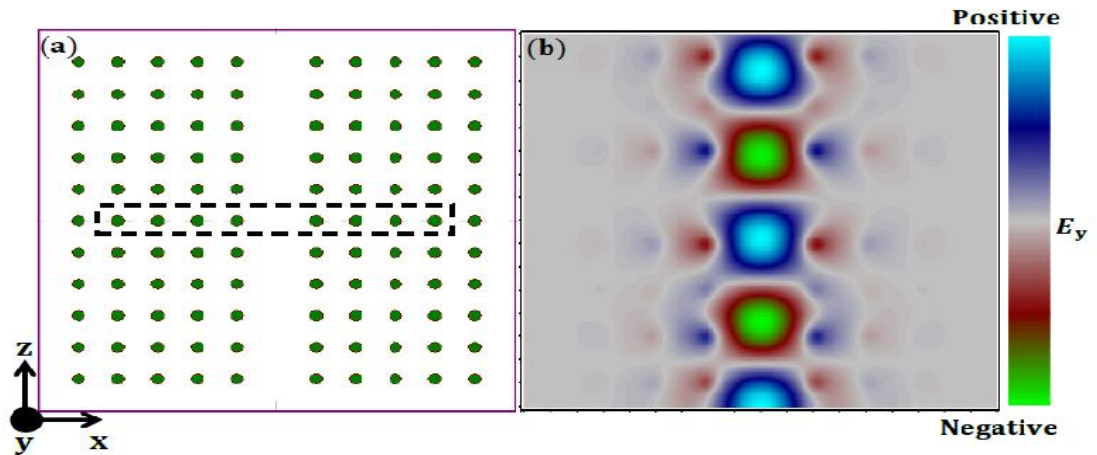


Figure 3.8: (a) demonstrates the 2D-PhC cross-section with a number of point defects. Within the periodic crystal, series of point defects were developed by removing the core column rods. Super-cell was labeled with a black dashed rectangle with x-direction lattice

3.4 Merits of Photonic Crystals

Compared to standard optical systems there are many benefits. Its primary benefit is the control of optical characteristics and light containment through structural design engineering. Some of the benefits are listed below:

- a) Photonic crystals reflect light of a specific range of wavelengths, resulting in one cavity mode unlike metal cavities. The metal represents the entire wavelength leading to infinite mode.
- b) It can resist elevated electrical fields.
- c) The size of photonic crystal instruments is in the order of light's wavelength. Therefore, the size of the devices is small.
- d) It processes the information at elevated velocity as the velocity of travel is the velocity of light in the structure.
- e) As the data carriers are photons unlike electrons in metallic cables, these instruments are resistant to short circuits as well as noise.
- f) Power usage is small compared to photonic crystal's linear property.
- g) Because of the big difference current for efficient index, it confines the light extremely in the structure.
- h) It regulates the lattice's spontaneous emission.

CHAPTER 4

SOFTWARE DESCRIPTION

4.1 RSoft Software

4.1.1 Basic 2D Simulation

This tutorial shows fundamental CAD layout characteristics through the creation of a new design file and shows a sample workflow to simulation performance and simulation outputs.

4.1.2 CAD Window Basics

They start by opening the window of the RSoft CAD. Users of Windows can do this through this Start menu and users of Linux may issue the `xbcad` command on such a command prompt. A window of the CAD displayed in Figure 4.1.1, The following components are included:

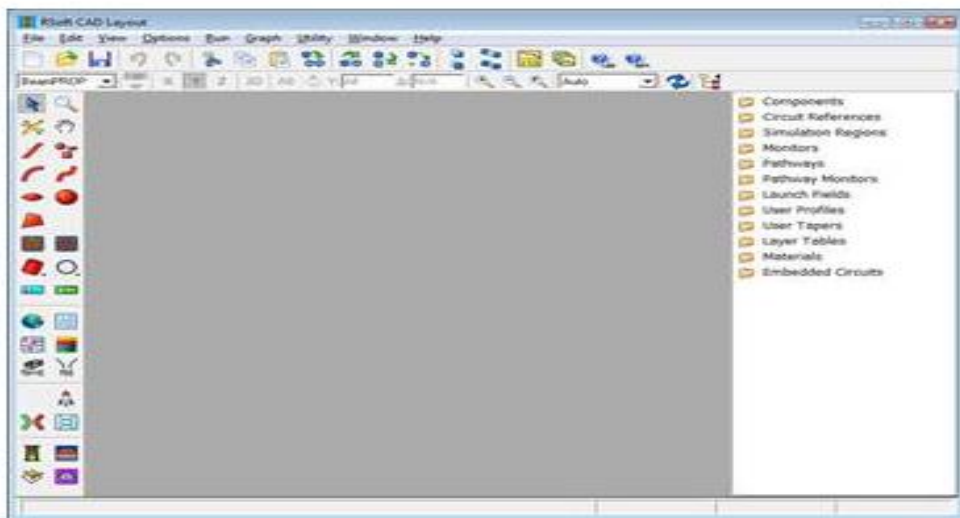


Figure 4.1: The RSoft CAD layout window, appearing the menu bar at the top, the top and left toolbars, and the status line at the bottom

The menu bar near the upper of the window-The menu bar allows access to a variety standard file and editing operations. The tree control on a the right of the window – Its tree control enables the viewer to readily access all the elements in the design, and other choices such as monitors, materials, tapers, profiles, etc.

4.1.2 Creating a New Design File

Tap the New Circuit button at the top toolbar to generate a fresh design document. Conversely, from the menu select File / New. Indicates the startup dialog as seen in Figure 4.2

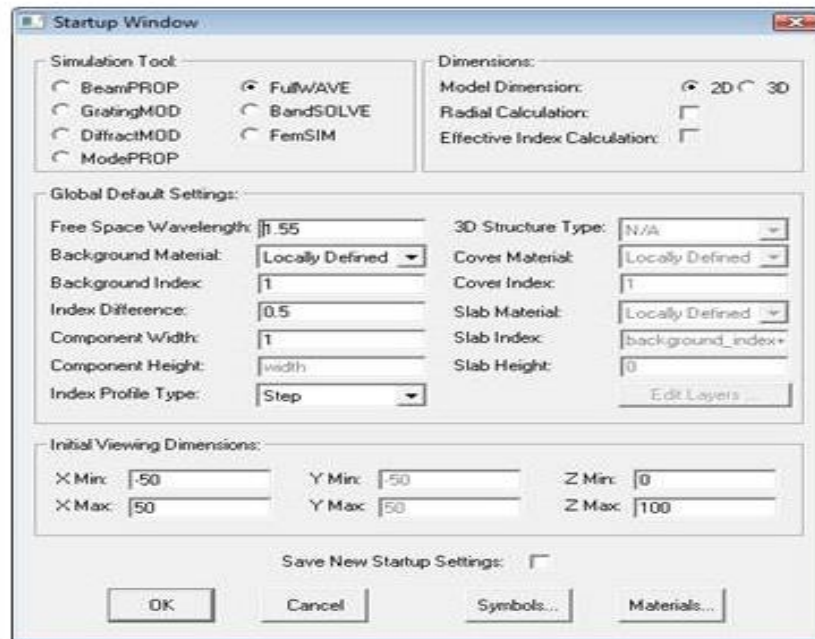


Figure 4.2: The startup dialog that appears whenever a new design file is created

The dialogue here require information about the structure that is to be modeled along with the background refractive index, wavelength of light and the default change in refractive index when the structure and background are considered. RSoft packages usually comprises of startup dialog however all its alternatives may not be of applicability when Fullwave is taken into consideration.

4.1.4 Selecting Initial Settings:

Once the settings are initialized, now it proceeds to the sub sequential stage. The Global settings can be managed with the aid of the 'Globe' icon present in the left end tool bar and adjustments can be made.

Table 4.1: Choosing Initial stage

Simulation tool used	Full Wave	Makes use of Full WAVE as simulation engine
Dimension of model	2D	2D simulation
Free space wavelength	1.55	Uses a fixed simulation wavelength [μm] used worldwide. This wavelength used represents the CW simulation driver wavelength and the middle wavelength when pulsed simulation is considered.
Background index	1	Represents the refractive index of the background material used before the actual implementation of the designed structure.
Index difference	0.5	Presents the variability that exists between the refractive indices of the background used and the implemented structure. This value is unique and in our structure the value evaluates to 1.5.
Component width	1	Describe the default component width in μm . Even though default, if desired components can be assigned with unique values.

4.1.5 The Layout Window:

Figure 4.3 shows the layout window that has been created using the primary CAD (Computer Aided Design) tool. The x and z axes are represented by lines that are light grey and the coarse coordinate grid by the dots. light grey and the coarse coordinate grid by the dots.

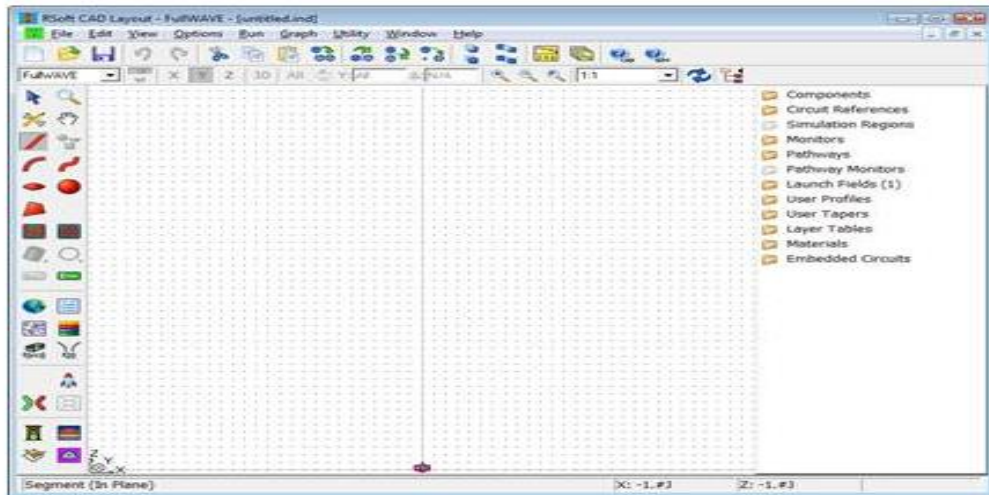


Figure 4.3: CAD Layout

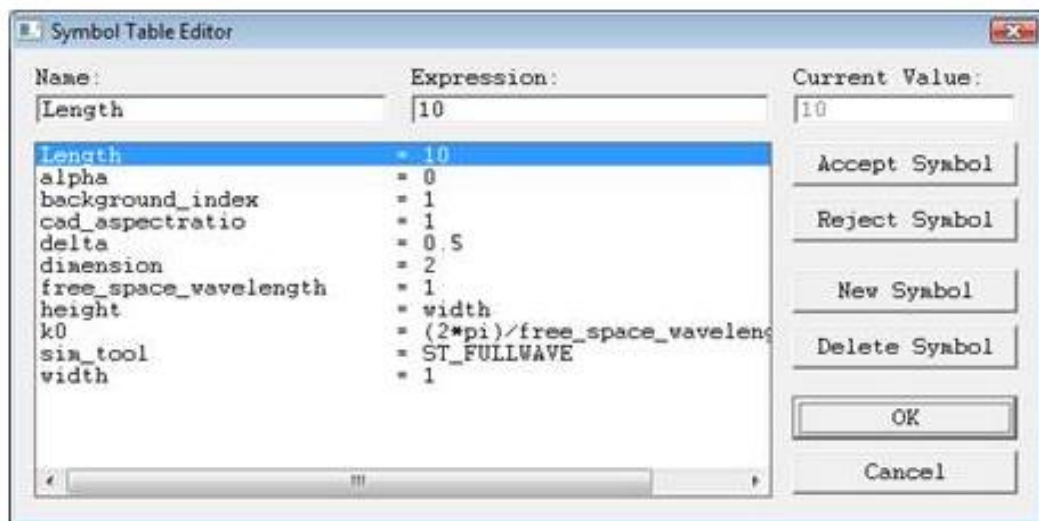


Figure 4.4: Symbol Table Editor: its variable Length with such a value of 10 was described.

We will generate the variable in every tutorial to set the length in our slab waveguide. Describe the Length of a sign and set this to 10. Click New Symbol to go there, enter a Name (Length) and Expression (10) symbols, but then click Accept Symbol. A Length variable must appear throughout the table of symbols.

4.1.7 Adding the Waveguide

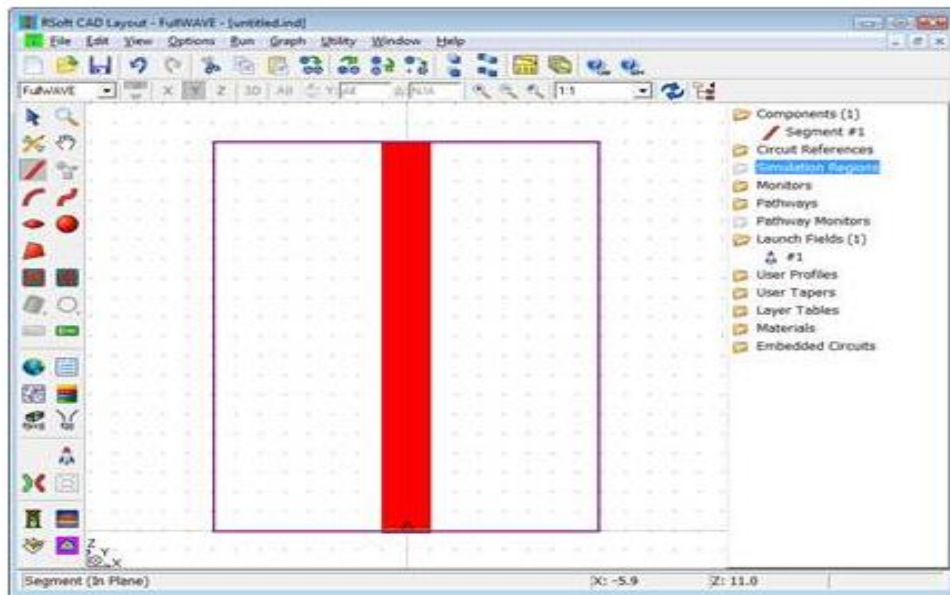


Figure 4.5: The straight segment since drawing because it appears. It shows a domain of simulation and also the field of launch.

4.1.8 Drawing the Waveguide:



Figure 4.6: Its segment characteristics dialog in the above model for the segment. Of this example, they will set the waveguide's length is 10 μm .

4.1.9 Choosing the Excitation

The basic mode of a waveguide element we developed should be this spatial element of our launch area. From this is a straightforward 2D slab design, an analytical mode solution could be computed by FullWAVE.

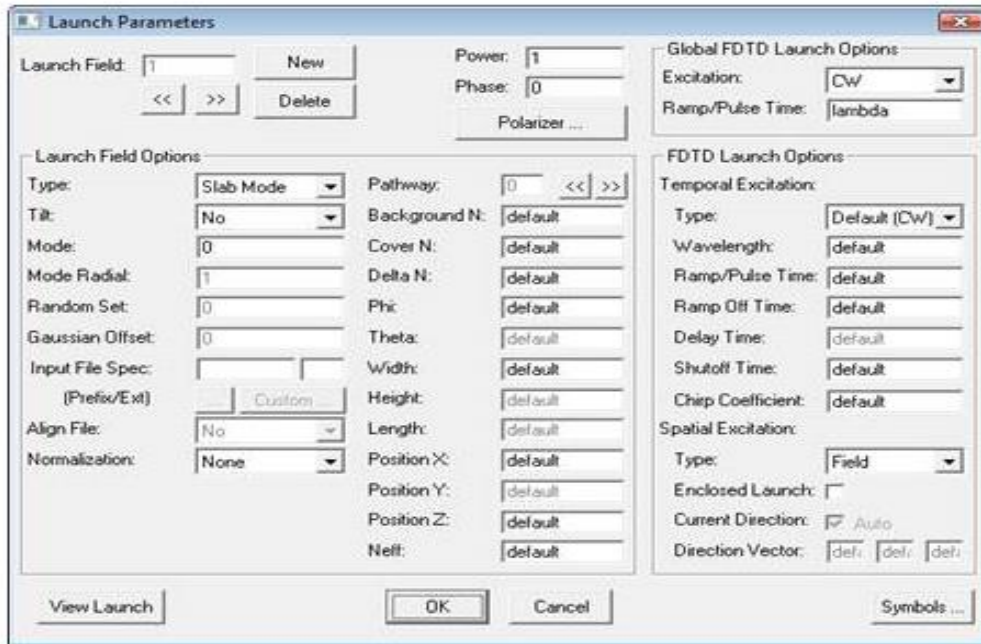


Figure 4.7: The Launch Parameters dialog.

Click an Edit Launch Field button throughout the left toolbar in the CAD to open the Launch Parameters dialog to set the launch field to an analytically computed mode profile.

Default start settings are suitable in this situation. Note the appropriate settings:

Option	Value	Description
Type	Slab Mode	It shows the need to launch an analytical slab mode
Mode	0	It suggests that the fundamental mode must be used.
Pathway	0 (unset)	A pathways used it calculate the launch field characteristics, including the efficient index, width and position of the launching slab

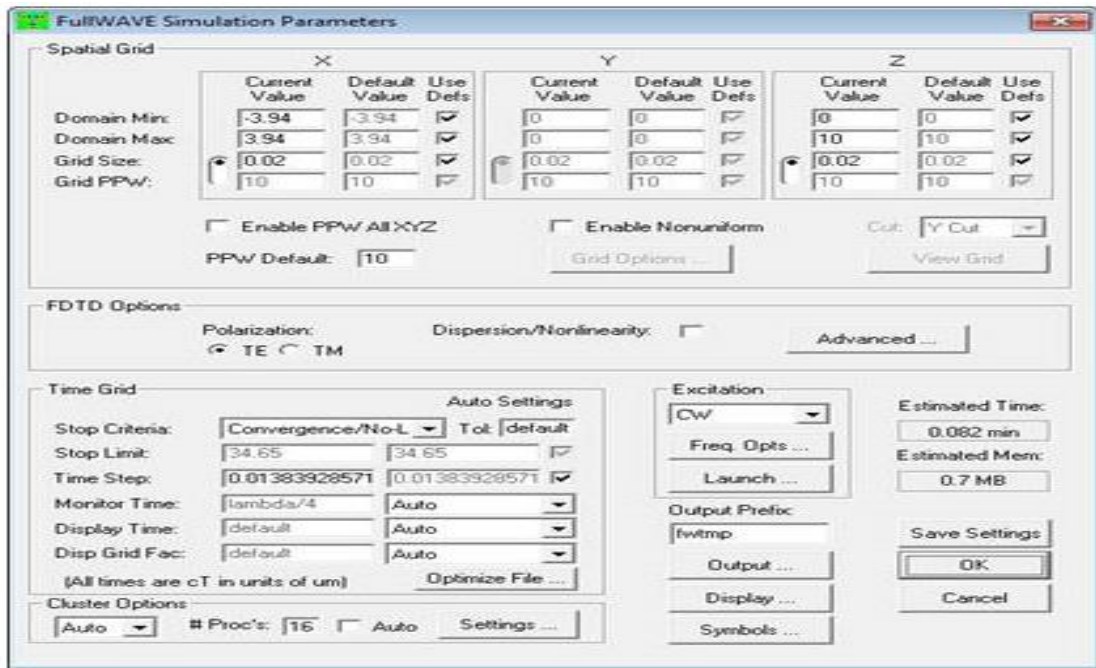


Figure 4.8: The FullWAVE Simulation Parameters dialog where the Default Launch settings are located.

4.1.10 Adding a Monitor

FullWAVE monitors activate readings of subsequent viewing or processing after a simulation.

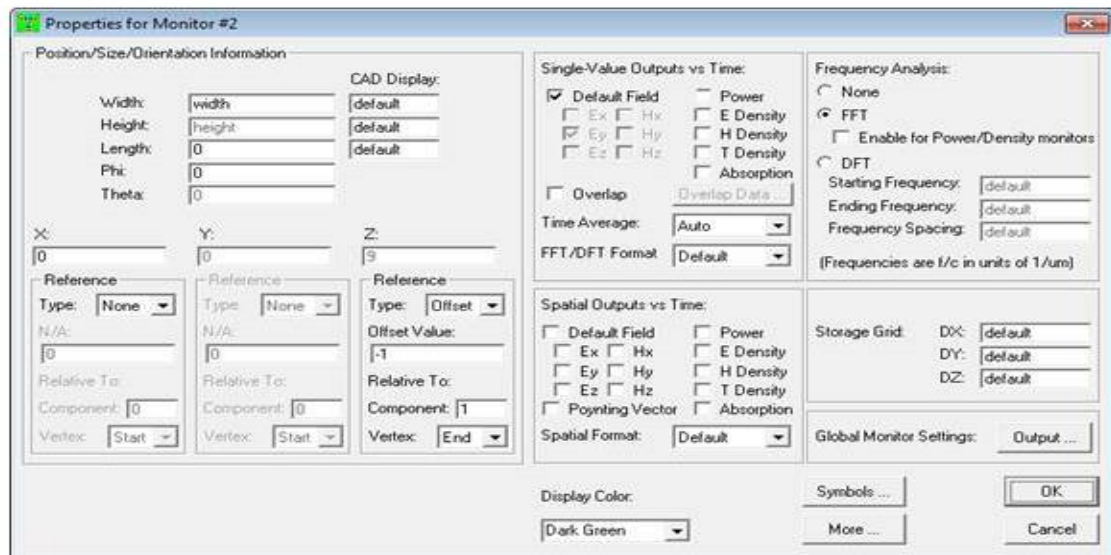


Figure 4.9: The properties dialog for a monitor.

To add a monitor to the layout, use the Monitor drawing mode in the left CAD toolbar. After drawing the monitor, right click on the monitor to open its properties dialog as shown in Fig.4.9. That dialog allows for many kinds of data to be saved as well as perform a frequency analysis.

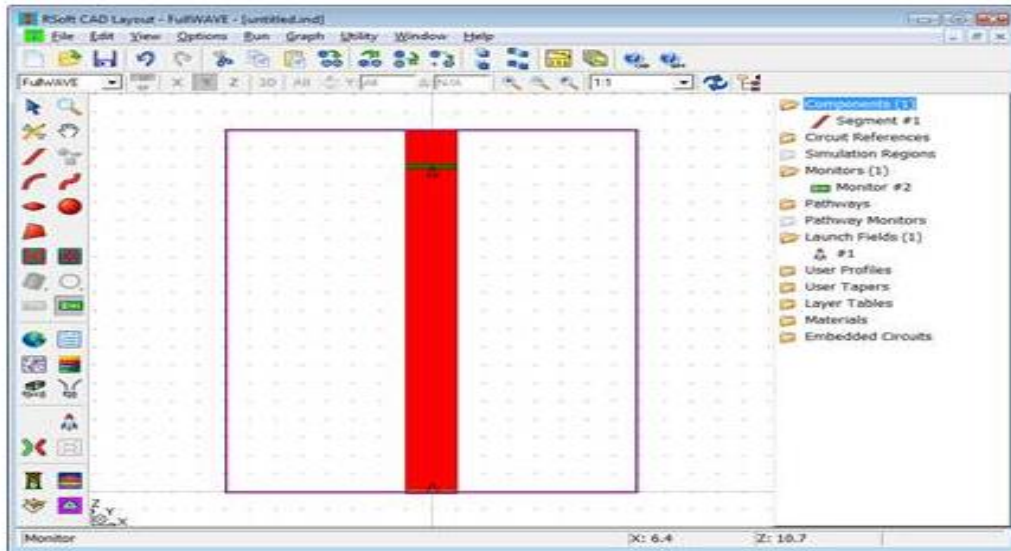


Figure 4.10: The completed structure in the CAD with the monitor created.

4.1.11 Performing the Simulation

By pressing its Perform Simulation button on a left toolbar to open the FullWAVE Simulation Parameters dialog, they can start a simulation when the layout or evaluation configuration is complete. It's the same dialog used to set parameters for a default release. They have to operate the simulation long sufficiently compute the directed energy so the field at the monitor reaches a stable state. Note that Convergence / No-Limit are set to a Stop Criteria, which suggests that the simulation can run until FullWAVE detects a stable state.

A calculation starts inside a new window distinct from the primary program when a simulation is launched, as seen in Figure 4.8.

4.1.12 The Simulation Window

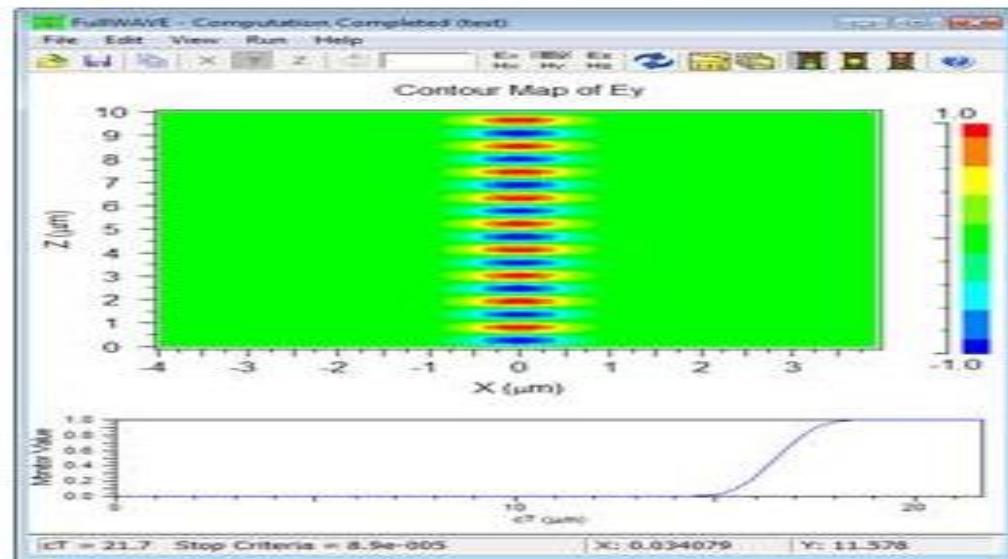


Figure 4.11: A distinct program in simulation after waveguide structure has been simulated. A graphic display demonstrates the optical field's color-coded contour plot

4.1.13 Accessing Saved Data

Both those FullWAVE saved information is in ASCII format, making it easy to access. Two files are created for most production: a raw data file or a command file for WinPLOT plotting which instructs when to show the information. Plotting command files generally get an extension starting with the 'p' character.

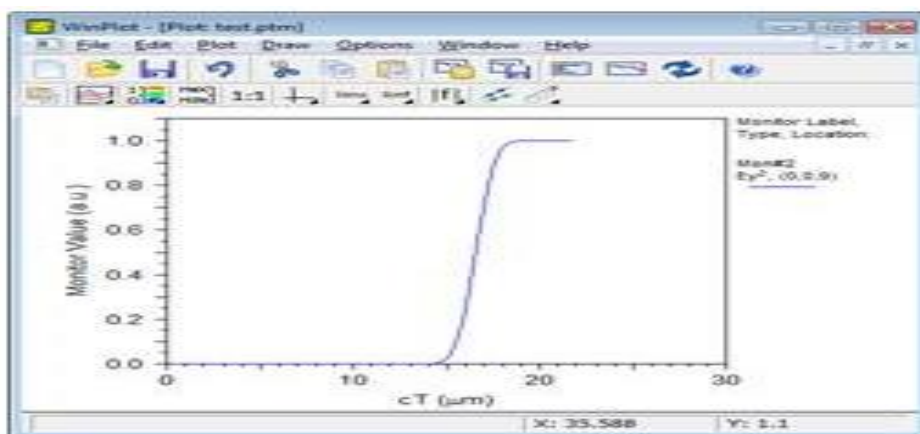


Figure 4.12: The WinPLOT window that demonstrates this simulation's monitor outcome.

4.1.14 Opening Plots

Click on a View Graphs icon in the upper toolbar of a CAD window to view the saved simulation outcomes, and pick the required graph from dialog shown. In this situation, there are several plotting files entered with the Output Prefix, including the test.ptm.

4.1.15 Viewing the Plotting Commands

The plotting command file test.ptm opened in WinPLOT is only a text file containing instructions for plotting. To view this file, either open it in a text editor or the WinPLOT window, press the View Editor button.

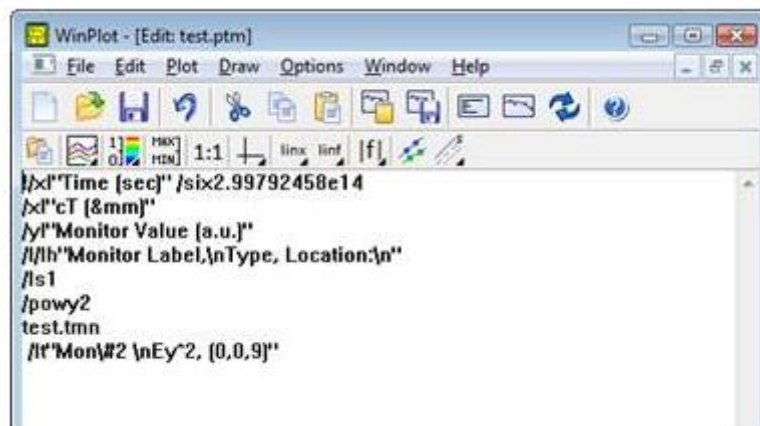


Figure 4.13: Viewing the Plotting Command

4.1.16 Viewing the Raw Data

The raw data file test.tmn may be opened in any text editor, and contains two columns: the first seen the time coordinates in units of μm (cT); the second appears the monitor result.

4.2 Operating Principle

In this project having three inputs, two outputs and one additional input is controlling input this controlling input creates phase between inputs by the interference principle [31]

4.2.1 Constructive Interference

Constructive interference is now a wave interference that happens as it meets one another in phase waves or creates a new wave to higher amplitude. As two-phase waves of the same frequency meet simultaneously at the same location, the two wave

amplitudes are simply added together. Resulting wave amplitude is higher than for the initial wave amplitude

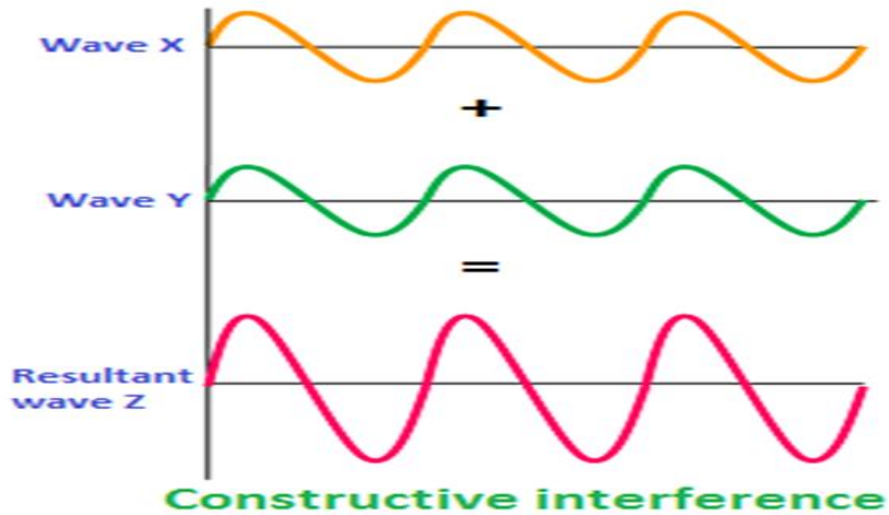


Figure 4.14: Constructive Interference

4.2.1 Destructive Interference

Destructive wave interference is a wave interference that happens when waves come together out of stage and form a new wave with reduced amplitude of zero.

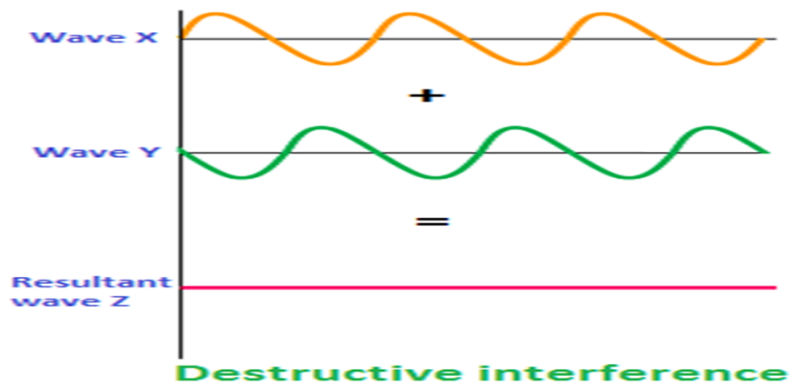


Figure 4.15: Destructive Interference

Two numerical techniques commonly used for designing and analyzing PhC's have been described in this section. These techniques are the plane wave expansion (PWE) and the FDTD. First method solves the equations of the Maxwell's in the frequency domain, while in the time domain the second method solves the same.

4.3 Numerical Analysis

4.3.1 Maxwell's equations

Four Maxwell equations govern the propagation of light through PhC's. These equations can be structured as follows in a source-free region [30].

$$\nabla \times H - \epsilon_0 \epsilon_r \frac{\partial E}{\partial t} = \sigma E \quad (4.1)$$

$$\nabla \times E + \mu_0 \mu_r \frac{\partial H}{\partial t} = -\rho H \quad (4.2)$$

$$\nabla \cdot E = 0 \quad (4.3)$$

$$\nabla \times H = 0 \quad (4.4)$$

Where

E: - Electric Field

H :- Magnetic Field

ρ : - Equivalent Magnetic Loss

σ : - Electric Conductivity

ϵ_r : - Relative permittivity

ϵ_0 : - Free space permittivity

μ_r : - Relative permeability

μ_0 : - Free space permeability

4.3.2 PWE Method

The PWE technique is commonly used to obtain dispersion relationships (frequency ν /s wave vector) and mode profiles within PhC constructions. This technique is common in the photonic crystal community as a technique of solving particular photonic crystal geometries for the band structure (dispersion relationship).

PWE is traceable to analytical formulations and is helpful in calculating Maxwell's modal alternatives over an inhomogeneous or regular geometry. It is specifically

tailored to address issues with non-dispersive media in a time-harmonic form. It is a technique of the frequency domain in which Bloch principle is used to address the issues of its own value and answers are acquired as a plane wave superposition. This technique does the calculations instead of the actual lattice in the related reciprocal lattice.

4.3.2.1 Derivation of PWE Method

Maxwell's equations is used in lossless medium (1) and (2) can be rewritten as

$$\nabla \times H(x, t) - \epsilon_0 \epsilon_r \frac{\partial E(x, t)}{\partial t} = 0 \quad (4.5)$$

$$\nabla \times E(x, t) + \mu_0 \mu_r \frac{\partial H(x, t)}{\partial t} = 0 \quad (4.6)$$

For most dielectrics, relative permeability (μ_r) is unity. Therefore, we have $\mu_r = 1$ in equation (6).

$$\nabla \times E(x, t) + \mu_0 \mu_r \frac{\partial H(x, t)}{\partial t} = 0 \quad (4.7)$$

We can discover alternatives in a time-harmonic form for the magnetic and electrical field:

$$H(x, t) = H(x) \exp(-i\omega t) \quad (4.8)$$

$$E(x, t) = E(x) \exp(-i\omega t) \quad (4.9)$$

It is possible to write curl equations (5) and (6) pertaining to electrical and magnetic fields as

$$\nabla \times H(x) + i\omega \epsilon_r(x) \epsilon_0 E(x) = 0 \quad (4.10)$$

$$\nabla \times E(x) - i\omega \mu_r(x) \mu_0 H(x) = 0 \quad (4.11)$$

Then divide Eq. (10) by $\epsilon_r(x)$ and then take the curl

$$\nabla \times \left(\frac{1}{\varepsilon_r(x)} \nabla \times H(x) \right) + iw\varepsilon_0 \nabla \times E(x) = 0 \quad (4.12)$$

Using Equation (11) in above given equation

$$\nabla \times \left(\frac{1}{\varepsilon_r(x)} \nabla \times H(x) \right) - w^2 \varepsilon_0 \mu_0 \nabla \times H(x) = 0$$

$$\nabla \times \left(\frac{1}{\varepsilon_r(x)} \nabla \times H(x) \right) = w^2 \varepsilon_0 \mu_0 \nabla \times H(x)$$

Putting $c = \frac{1}{\sqrt{\varepsilon_0 \mu_0}}$ in equation (12)

$$\nabla \times \left(\frac{1}{\varepsilon_r(x)} \nabla \times H(x) \right) = \left(\frac{w}{c} \right)^2 H(x) \quad (4.13)$$

Therefore, we can write an electric field equation

$$\frac{1}{\varepsilon_r(x)} \nabla \times (\nabla \times E(x)) = \left(\frac{w}{c} \right)^2 E(x) \quad (4.14)$$

Eq. (13) and (14) are instances of issues of own value with $\left(\frac{w}{c} \right)^2$ as their own values.

Particular equations is solved in order to achieve the Eigen-frequencies for the dielectric constant $\varepsilon_r(x)$. Eigenvectors equal to the proprietary frequency provide the pre profile data. We now consider the structure to be infinitely regular.

4.3.3 FDTD Method

Kane Yee suggested the FDTD technique in 1966 to fix a selection of electromagnetic issues. Several improvements or changes to the Yee's algorithm have been made since then to enhance power and reliability. They limit themselves to Yee's formula, which is best adapted to electromagnetics issues, in which Maxwell's curl equations are evaluated in the time domain to have easy alternatives.

4.3.3.1 Derivation of FDTD

Method 1 refers to the curl equation described by Maxwell in paragraph 4.3.1. E and H will have three field parts in a Cartesian coordinate system, i.e. E_x , E_y , E_z and H_x , H_y , H_z , including both. We can write six paired equations on the grounds of equations (1) and (2) as described below [31]:

$$\frac{\partial E_x}{\partial t} = \frac{1}{\varepsilon} \left(\frac{\partial H_z}{\partial y} - \frac{\partial H_y}{\partial z} - \sigma E_x \right) \quad (4.15)$$

$$\frac{\partial E_y}{\partial t} = \frac{1}{\varepsilon} \left(\frac{\partial H_x}{\partial z} - \frac{\partial H_z}{\partial x} - \sigma E_y \right) \quad (4.16)$$

$$\frac{\partial E_z}{\partial t} = \frac{1}{\varepsilon} \left(\frac{\partial H_y}{\partial x} - \frac{\partial H_x}{\partial y} - \sigma E_z \right) \quad (4.17)$$

$$\frac{\partial H_x}{\partial t} = \frac{1}{\mu} \left(\frac{\partial E_y}{\partial z} - \frac{\partial E_z}{\partial y} - \rho E_x \right) \quad (4.18)$$

$$\frac{\partial H_y}{\partial t} = \frac{1}{\mu} \left(\frac{\partial E_z}{\partial x} - \frac{\partial E_x}{\partial z} - \rho E_y \right) \quad (4.19)$$

$$\frac{\partial H_z}{\partial t} = \frac{1}{\mu} \left(\frac{\partial E_x}{\partial y} - \frac{\partial E_y}{\partial x} - \rho E_z \right) \quad (4.20)$$

CHAPTER 5

DESIGN PROCEDURE AND OPTIMIZATION

5.1 Design Procedure

The full adder design takes the form of two components, the first step is a CARRY preceded with an output phase as seen in Figure 5.2. The design comprise of three input ports, A, B and C, and one additional input port named controlling input (D_i) but two output ports, SUM and CARRY. The FA adds three binary 1-bit binary numbers and produce 2 outputs SUM as well as CARRY. From figure 5.1 the FA is effectively two half adder, an XOR and an AND gate, connected by an OR gate. The output at the port SUM is the combination full-adder logic are XOR between A, B and C and output of CARRY are the three AND gate combined by OR gate simultaneously, and the T-T is seen in Figure 5.4. As seen from the T-T of a full adder the (a) if all inputs are same then SUM equals CARRY (b) if two of inputs are zero then SUM equals one and CARRY is invers of (c) if two of inputs are one then CARRY equals one and SUM is inverse of it. Light intensity is regarded as logic '1' in many of the indicated PhC-based logic gates and no light or zero light intensity is regarded as logic '0'. An additional input (D_i) creates phase between inputs.

The indicated full adder lattice structure is shown in Figure 5.2 where the CARRY will be the first phase of both the ports but the next process is the output phase. Light beam interference occurs at the input and output phases of T-junctions. At the T-junction of the CARRY level, input light coming from ports A, B and C are allowed to interfere and directed to both the output level T-junction. For $A = B = C = 1$ input combinations, the output produced both SUM as well as CARRY and controlling input considers as 0° phase because of constructive interference.

To other input pairs such as B, the light beam from in the correlating port will be targeted at the T-junction of the output level with less light reflected by the edge segment re_1 in the living in poverty input port. At input C edge rod re_2 control both CARRY and SUM outputs. For destructive interference between all input combination phases and controlling input, the phase is 180° . And for constructive interference between all input combination phases and controlling input phase is 0° . From the figure 5.2 the structure composed of 15×31 array of cylindrical holes of Si

material with the refractive index of 3.46. The band diagram of this system is computed using a PWE method showing three PBG as seen in Figure 5.3, two for TE mode and another for TM mode.

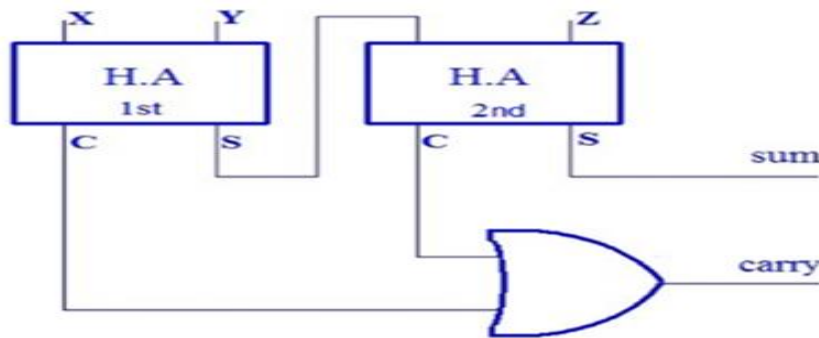


Figure 5.1: Combinational circuit diagram of Full Adder

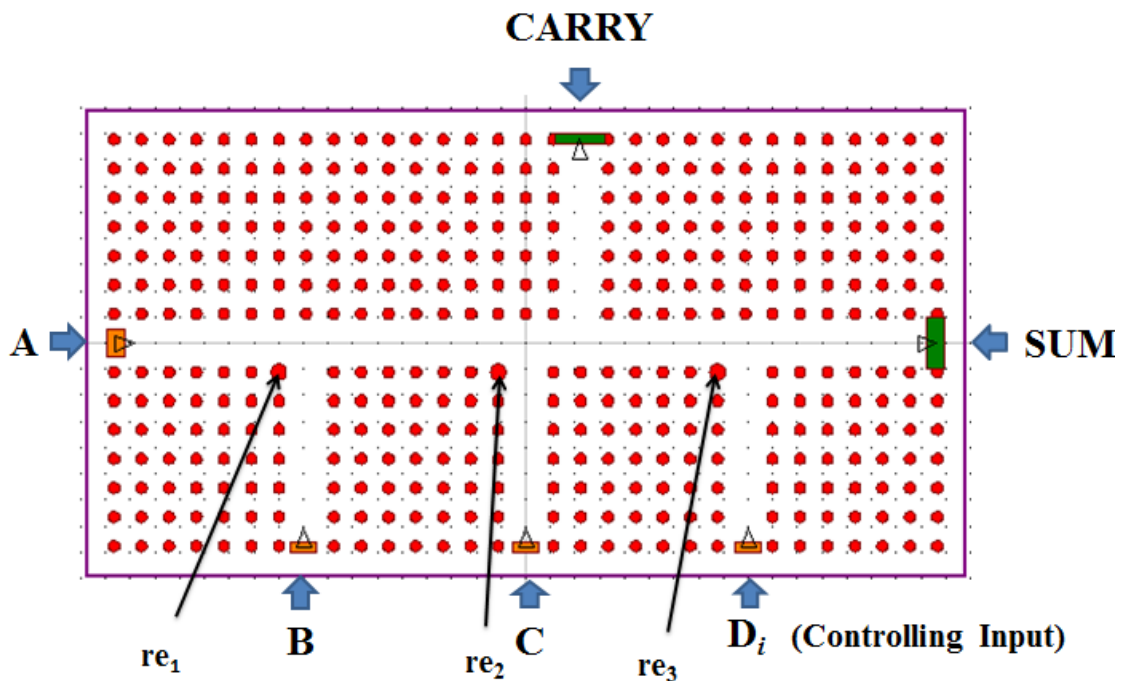


Figure 5.2: Lattice structure for Full Adder

The lattice constant a is set to 555 nm to adjust any of the TE PBGs for the display of the optical telecommunications. The band gap appropriate for this implementation varies from 0.27558 (a/λ) to 0.44302 (a/λ) that meaning that the present structure enables wavelength light from 1.26 μm to 2.05 μm . Every Si rod's radius is 0.2a as

well as the re_1 , re_2 and re_3 rod radii are optimized to $0.27 a$, $0.275 a$ and $0.288 a$ respectively. With 31×15 Si rods array with square lattice, T-shaped waveguides were created for both stages.

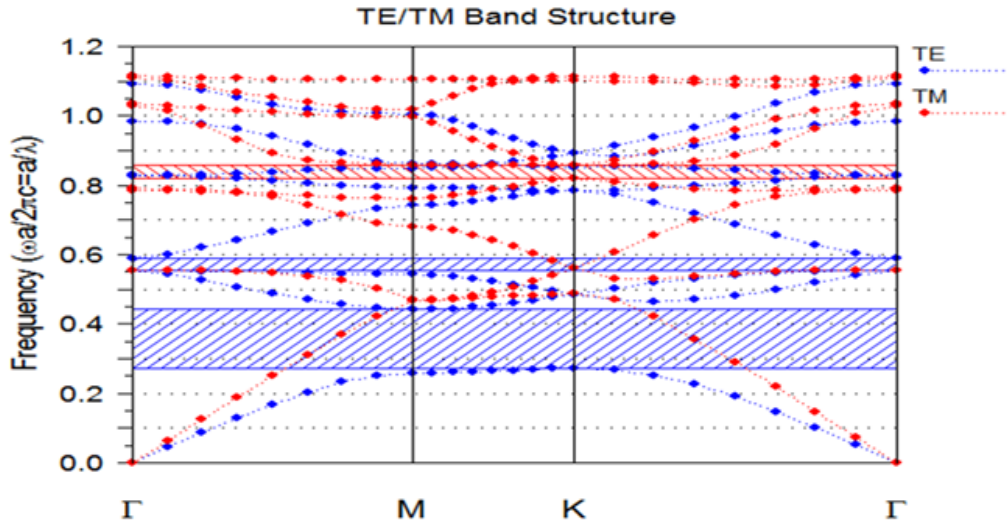


Figure 5.3: Band diagram for FA structure

Table 5.1: Truth Table for FA

A	B	C	SUM	CARRY
0	0	0	0	0
0	0	1	1	0
0	1	0	1	0
0	1	1	0	1
1	0	0	1	0
1	0	1	0	1
1	1	0	0	1
1	1	1	1	1

5.2 Analysis on the basis of optimization of edge rods re_1 , re_2 and re_3

Optimized edge rod re_1 at port B because of obtained high contrast ratio and reduce reflection as seen in figure 5.2. Optimized edge rods reduce back reflection for not applied input meant zero input. Light travels by the four waveguides and observe the light red light and blue light intensity is more red light shows the upper part of the

sinusoidal cycle and blue part shows the lower part of the sinusoidal cycle [5]. And by the controlling input to invert this incoming light by the out of phase

After performing optimization calculating contrast ratio for obtained outputs. Logic '1' represents the light intensity and no light represents the logic '0'. If I am not done optimization then observe that obtained low contrast ratio after optimization increase contrast ratio.

CHAPTER 6

RESULT AND ANALYSIS

The proposed structure is simulated analytically and uses the FDTD method. At the wavelength of 1550 nm, a Gaussian standard profile CW light input P_a was introduced. To all output combinations, that output optical field distribution (OFD) spectrum is shown in Figure 6.1. Output power levels (OPL) for the sum and carry are presented in Fig. 6.2. The calculation of response time depends on both SUM and CARRY ports because the whole linear material impacts the structure implemented. As there was no input light applied (i.e., A, B, and C evaluates to 0), its input D_i finds no insight light to interfere too, but less part of that light input from D_i is consumed by a rod re_3 as it behaves as something of a cavity.

6.1 Optical Field Results

6.1.1 Simulation Results for A = 0, B = 0, and C = 1

From figure 6.1.1 the light's OFD for varying input combinations (A = 0, B = 0 and C = 1), along with the input D_i phase which is 0° allows for constructive interference and output to be produced at a SUM port, which is considered here as logic '1' state and most of the light appears at SUM port of the design

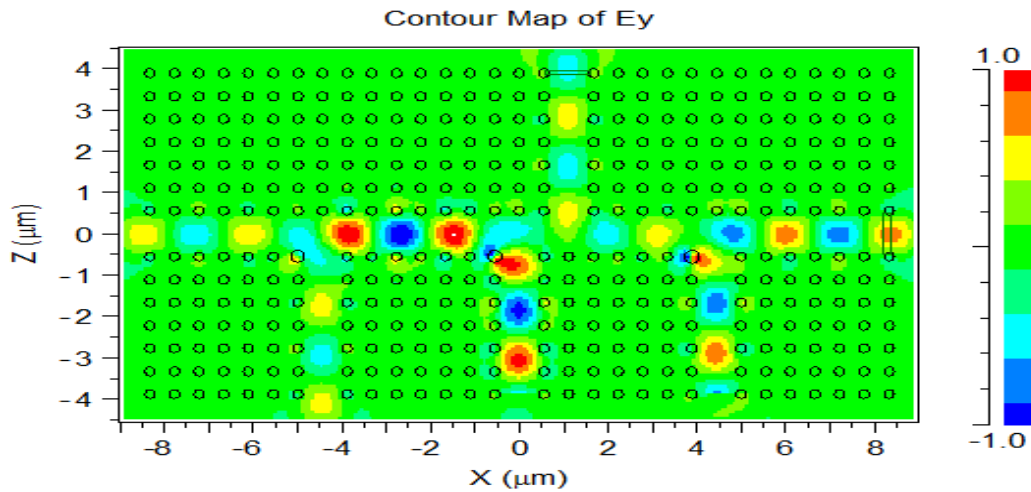


Figure 6.1: OFD for chosen input combinations A= 0, B = 0, and C = 1.

As more light appears at the SUM port, less light appears (considered as negligible that is power less than $0.5 P_a$) at the CARRY port, which is considered as logic '0'.

6.1.2 Simulation Results for $A = 0$, $B = 1$, and $C = 0$

Similarly, from figure 6.1.2 the OFD for the predefined input combination gets applied, and along with the input D_i phase which is 0° allows for constructive interference and output to be produced at a SUM port, regarded here as the high state, logic '1'. Hence major part of the light appears at the SUM port leading to lesser light appearing (considered as the negligible power that is less than $0.5 P_a$) at the CARRY port, which is considered as logic '0'.

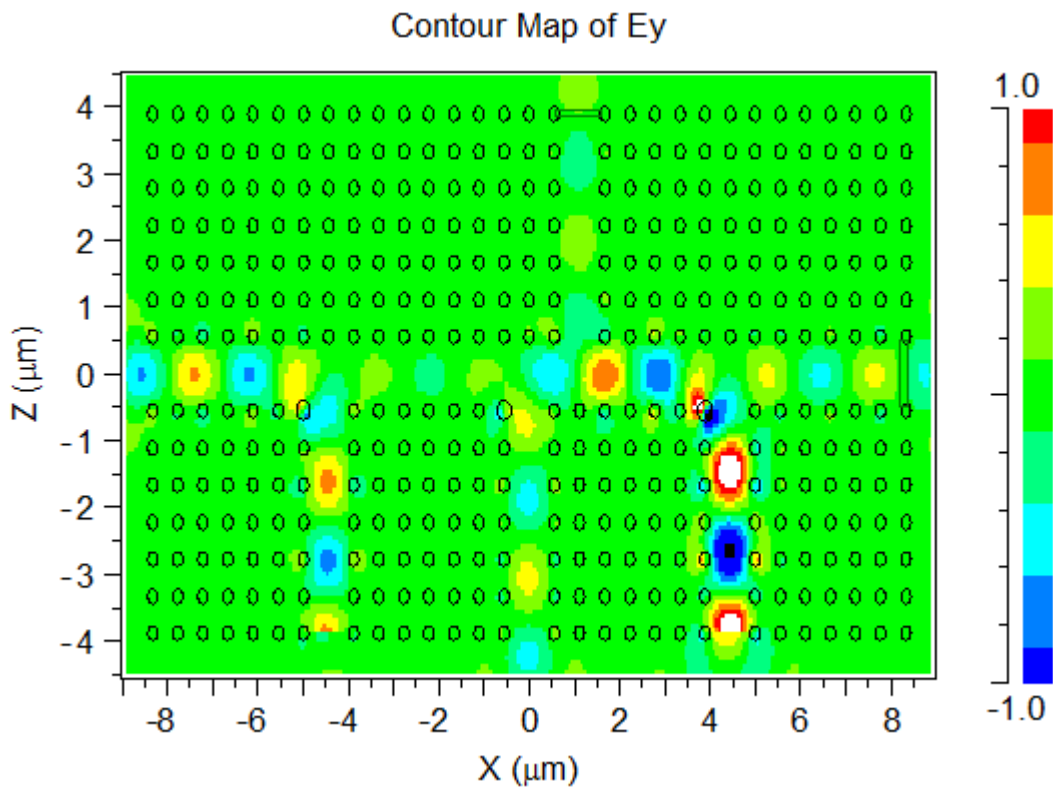


Figure 6.2: OFD for input combinations $A = 0$, $B = 1$, and $C = 0$.

6.1.3 Simulation Results for $A = 0$, $B = 1$, and $C = 1$

Similarly, from figure 6.1.3 its OFD for the light is applied for input combinations ($A = 0$, $B = 1$ and $C = 1$), and also the input D_i phase which is 180° allows for destructive interference and output to be produced at a CARRY port, which is regarded as logic '1'. Most of the light appears at the CARRY port. Less light appears (considered as negligible power that is less than $0.5 P_a$) at the SUM port, which is considered as logic '0'.

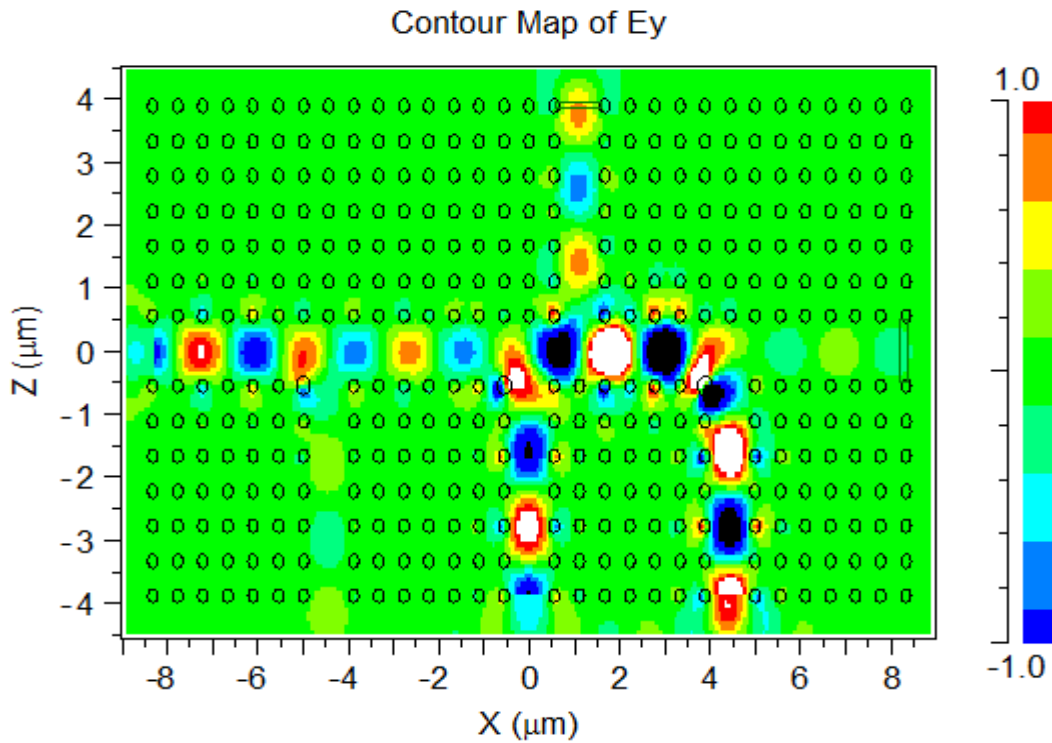


Figure 6.3: OFD for input combinations A= 0, B= 1, and C=1.

6.1.4 Simulation Results for A = 1, B = 0, and C = 0

Similarly, from figure 6.1.4 the OFD for the predefined input combination gets applied, and along with the input D_i phase which is 0° allows for constructive interference and output to be produced at a SUM port, regarded here as the high state, logic '1'. Hence major part of the light appears at the SUM port leading to lesser light appearing (considered as the negligible power that is less than $0.5 P_a$) at the CARRY port, which is considered as logic '0'.

6.1.5 Simulation Results for A = 1, B = 0, and C = 1

Similarly, from figure 6.1.5 its OFD for the light is applied for input combinations (A = 1, B = 0 and C= 1), and also the input D_i phase which is 180° allows for destructive interference and output to be produced at a CARRY port but is regarded as logic '1' most of the light appears at the CARRY port.

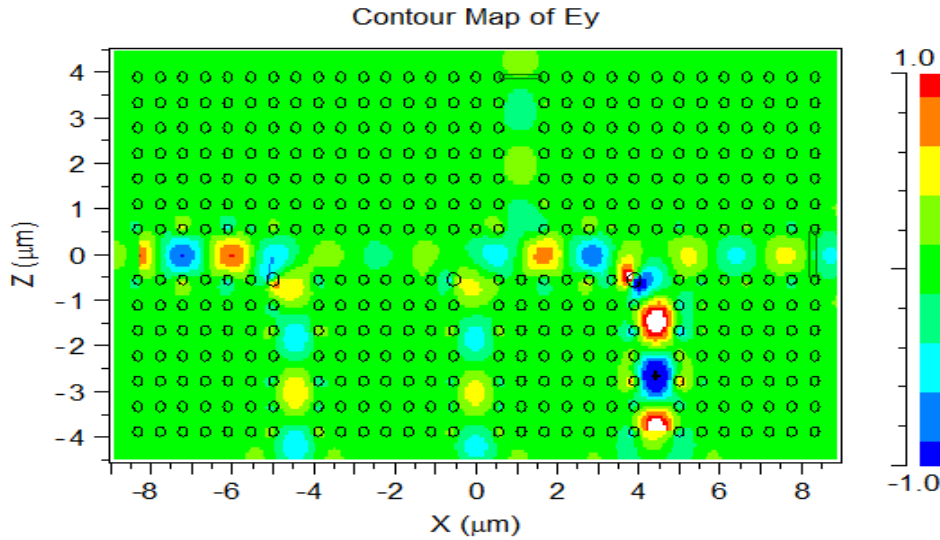


Figure 6.4: OFD for input combinations $A = 1$, $B = 0$, and $C=0$.

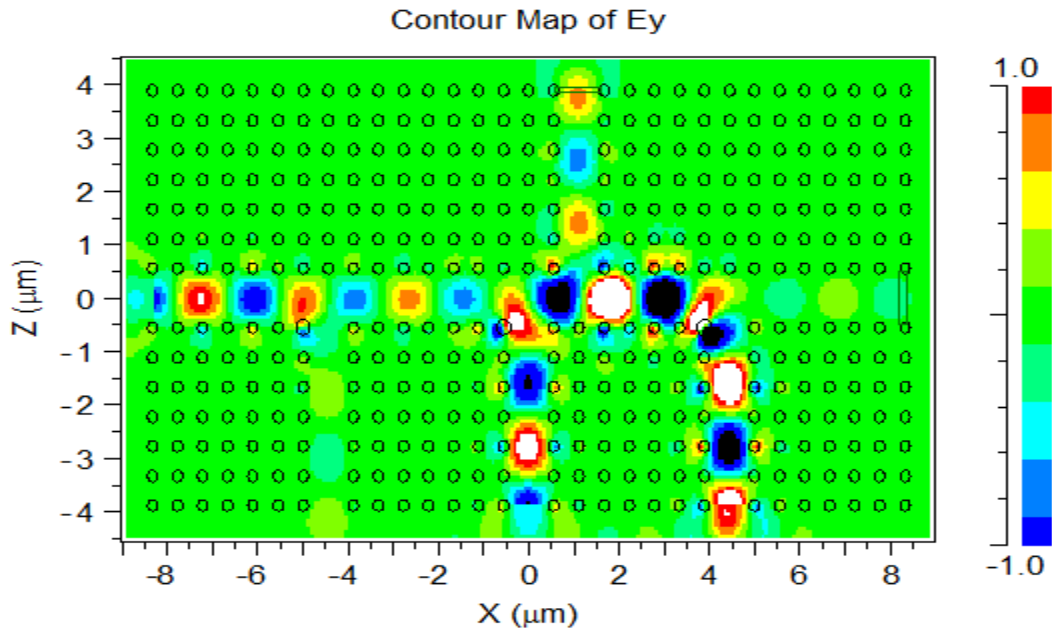


Figure 6.5: OFD for input combinations $A=1$, $B = 0$, $C=1$

Less light appears (considered as negligible power that is less than $0.5 P_a$) at the SUM port, which is considered as logic '0'.

6.1.6 Simulation Results for $A = 1$, $B = 1$, and $C = 0$

Similarly, From figure 6.1.6 its OFD for the light is applied for input combinations ($A = 1$, $B = 1$, and $C=0$), and also the input D_i phase which is 180° allows for destructive interference and output to be produced at a CARRY port which is considered as logic

'1' most of the light appears at the port CARRY. Less light appears (considered as negligible power that is less than $0.5 P_a$) at the SUM port, which is considered as logic '0'.

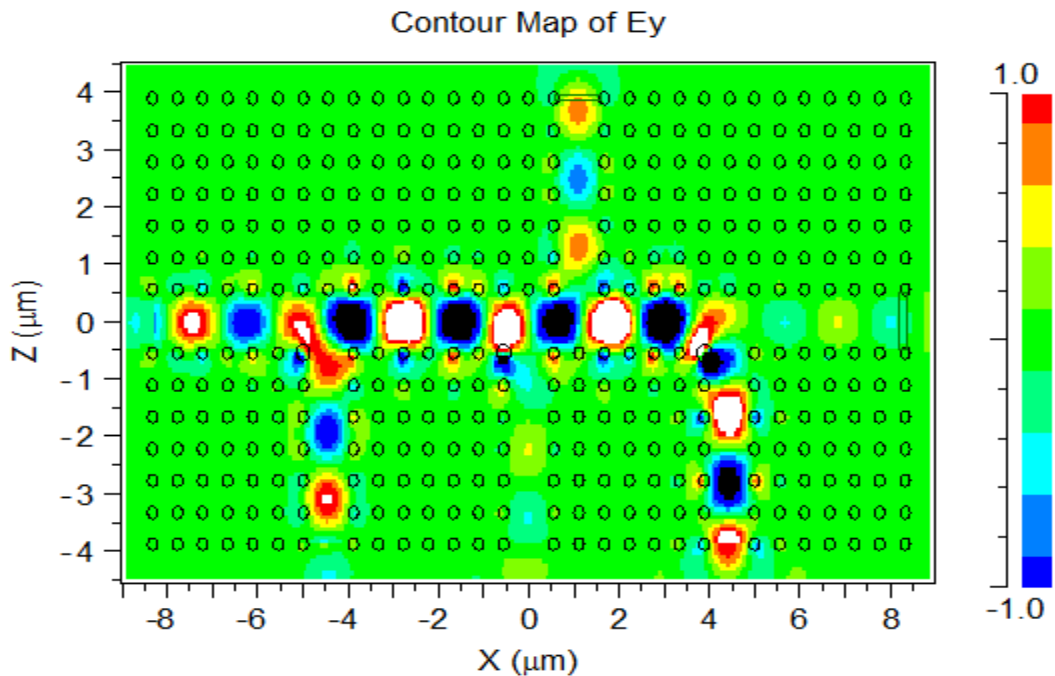


Figure 6.6: OFD for input combinations $A=1$, $B=1$, $C=0$

6.1.7 Simulation Results for $A=1$, $B=1$, and $C=1$

Similarly, from figure 6.1.7 its OFD for light is applied for all the input combinations ($A=1$, $B=1$ and $C=1$), and also the input D_i phase which is 0° allows for constructive interference and output to be produced at a SUM port which is considered as logic '1'. In this input combination Most of the light at port SUM is concentrated leading to the absence of waveguide bend. Less light is provided for the CARRY port, in comparison with SUM port which is assumed to be logic '1' because of greater than $0.5 P_a$.

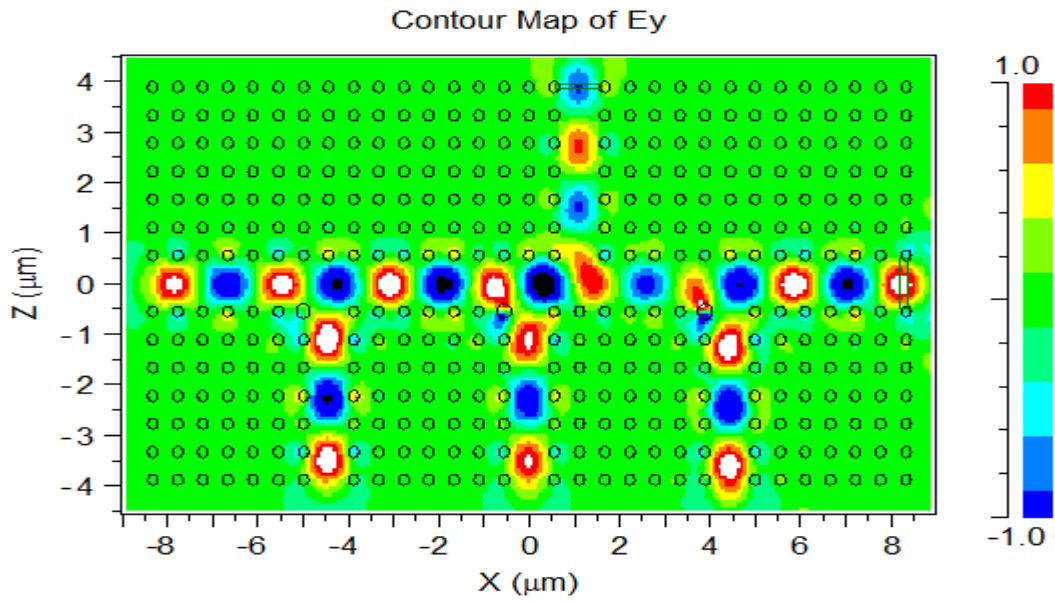


Figure 6.7: OFD for input combinations A = 1 , B = 1, C =1

Table 6.1: Proposed Full Adder: summary of CR

Input combinations			SUM outputs			CARRY outputs		
A	B	C	P_{out} / P_{in}	Min. CR(dB)	logic	P_{out} / P_{in}	Min. CR(dB)	logic
0	0	1	0.93		1	0.49		0
0	1	0	0.56		1	0.24		0
0	1	1	0.13		0	0.68		1
1	0	0	0.59	12.5	1	0.28	6.5	0
1	0	1	0.12		0	0.64		1
1	1	0	0.21		0	0.71		1
1	1	1	2.16		1	1.08		1

6.2 Optical Power Levels Of Sum And Carry Outputs

In given optical power levels that if average power greater than 0.5Pa than then considered as logic '1'and if average power less than 0.5 Pa then considered as logic '0' .

6.2.1 A = 0 , B = 0 and C = 1

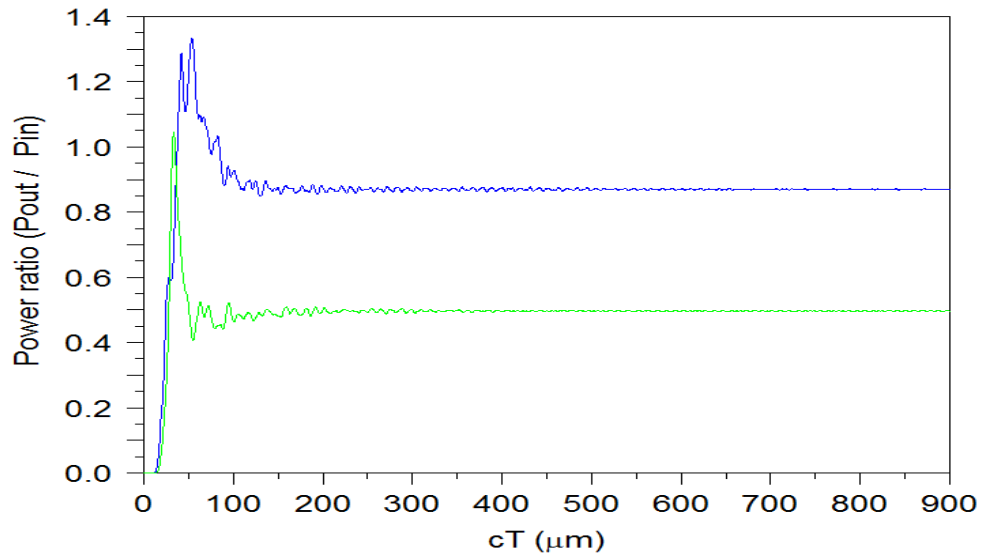


Figure 6.8: OPL at the ports SUM and CARRY for the input combinations A = 0 , B = 0 , and C = 1 (blue – SUM, green - CARRY)

From the table 6.1 observed that calculate minimum CR for the port SUM and port CARRY by .Contrast ratio defines the ratio high power to low power. Means ratio of logic '1' power to logic '0' for both of the outputs sum as well as the carry. **CR= 10 log P₁/P₀** represents P₁ is the power of logic 1 and P₀ represents the power of logic 0. Logic 1 represents the light intensity and no light represents the logic 0. From the port SUM Power for logic '1' = 2.16 Pa and for logic '0' = 0.12 Pa and for port CARRY power for logic '1' = 1.08 Pa and logic '0' = 0.24Pa.

The minimum value of the contrast ratio acquired at a SUM and CARRY ports respectively is 12.5 dB and 6.5 dB. Although the contrast ratio is relatively lower than that of the current full-adder models, the response time for the inputs and also their independence from non-linear material has rendered the suggested one superior over

6.2.2 A = 0, B = 1 and C = 0

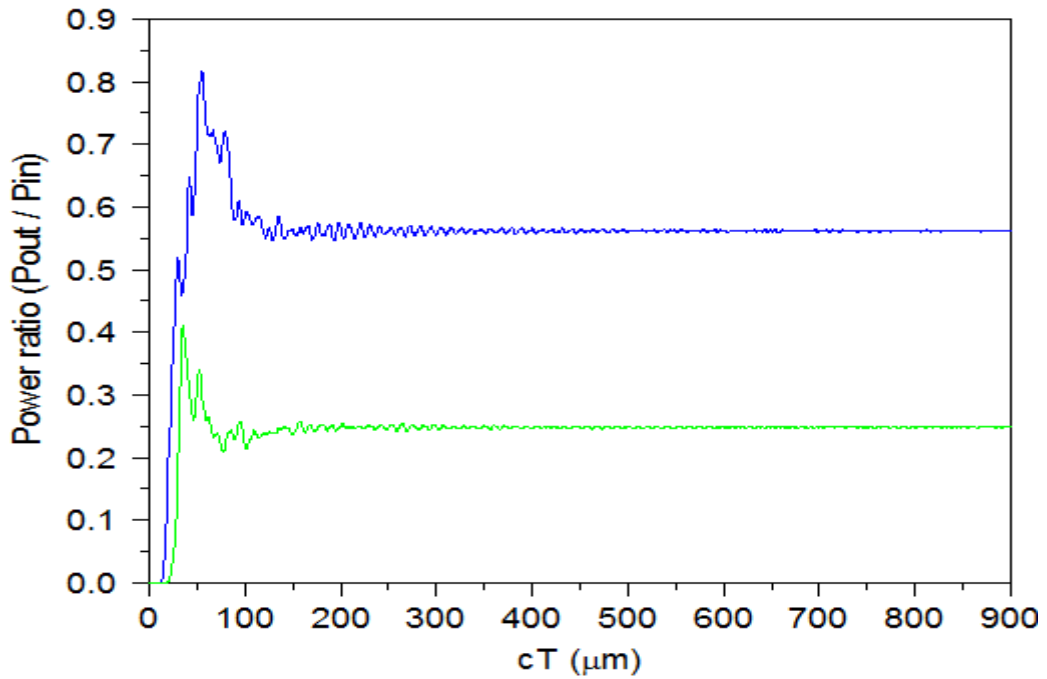


Figure 6.9: OPL at the ports SUM and CARRY for the input combinations A = 0 , B = 1 , and C = 0 (blue – SUM, green - CARRY)

6.2.3 A = 0, B = 1 and C = 1

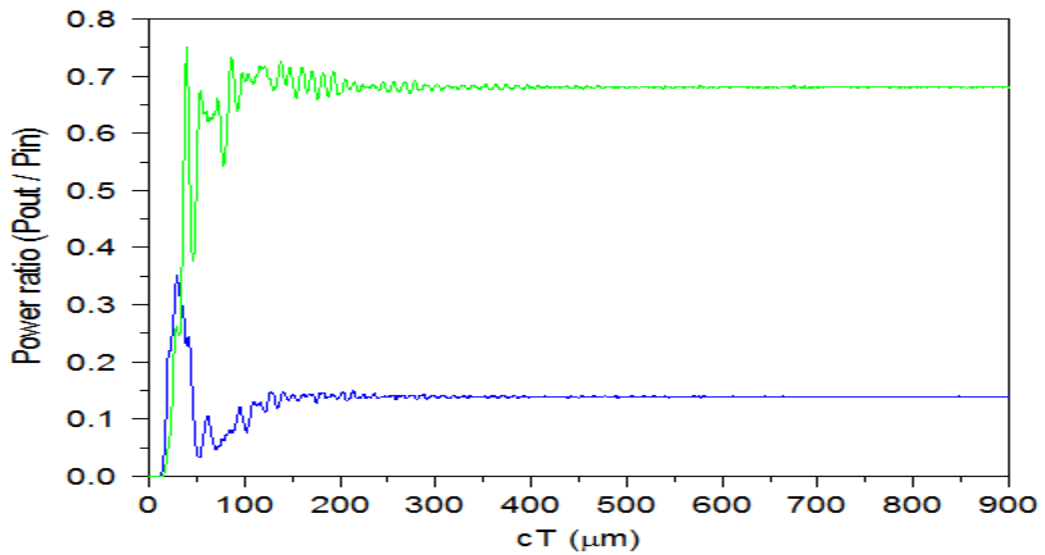


Figure 6.10: OPL at the ports SUM and CARRY for the input combinations A = 0, B = 1, and C = 1 (blue – SUM, green – CARRY)

6.2.4 A = 1, B = 0 and C = 0

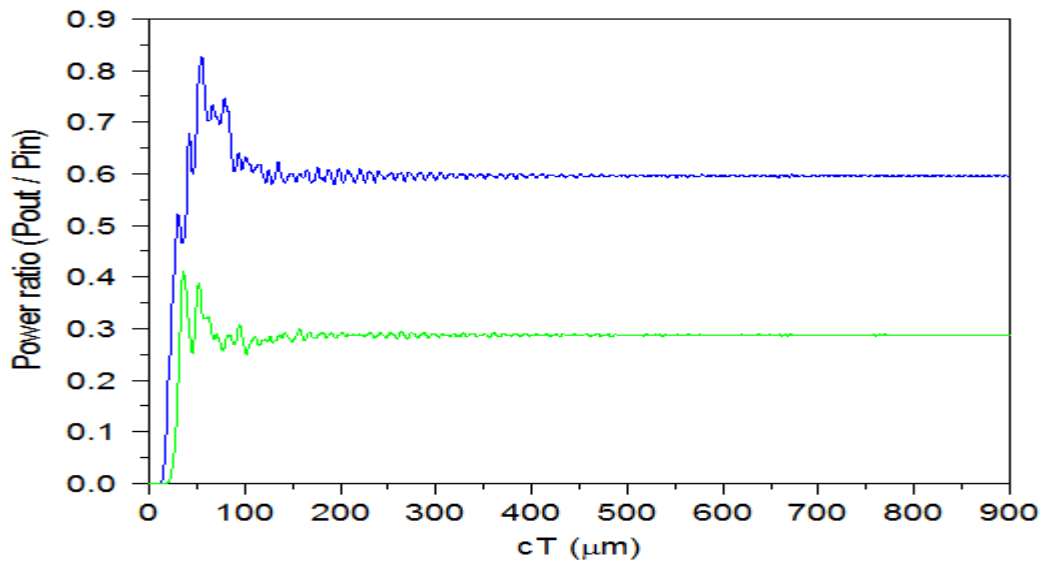


Figure 6.11: OPL at the ports SUM and CARRY for the input combinations $A = 1$, $B = 0$, and $C = 0$ (blue – SUM, green – CARRY)

6.2.5 A = 1, B = 0 and C = 1

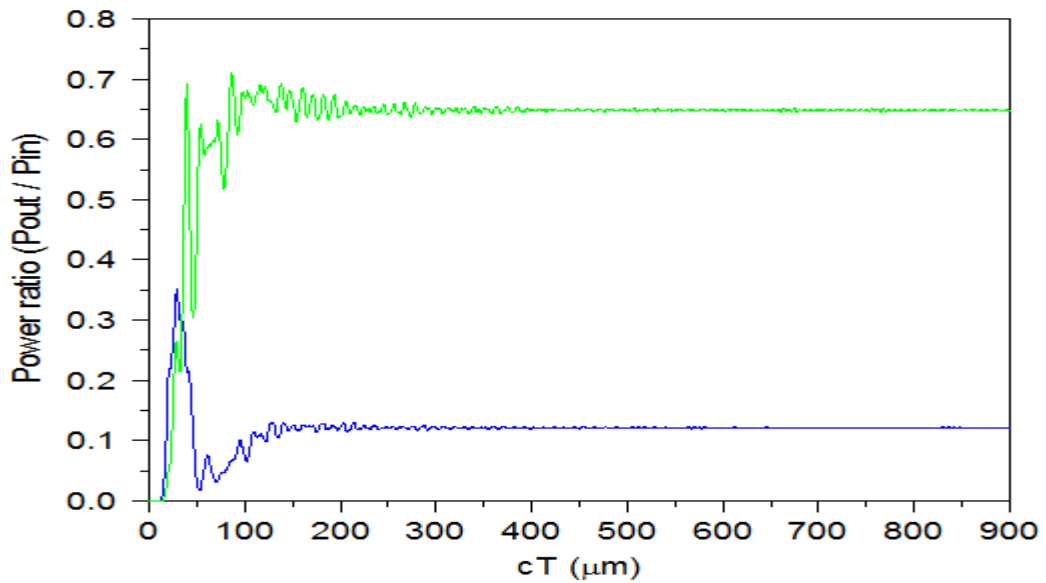


Figure 6.12: OPL at the ports SUM and CARRY for the input combinations $A = 1$, $B = 0$, and $C = 1$ (blue – SUM, green – CARRY)

6.2.6 A = 1, B = 1 and C = 0

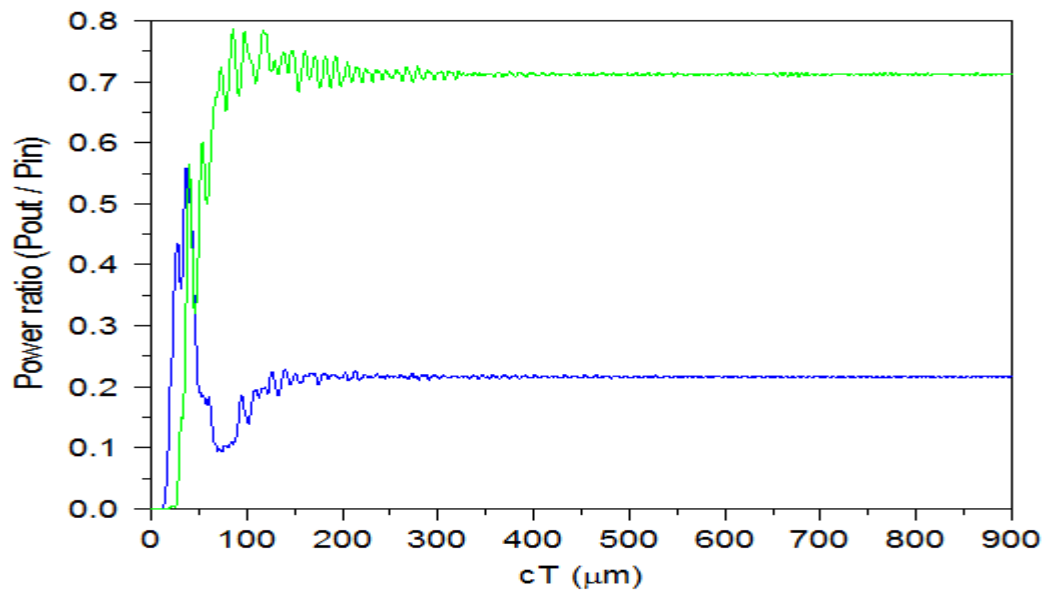


Figure 6.13: OPL at the ports SUM and CARRY for the input combinations A = 1

6.2.7 A = 1, B = 1 and C = 1

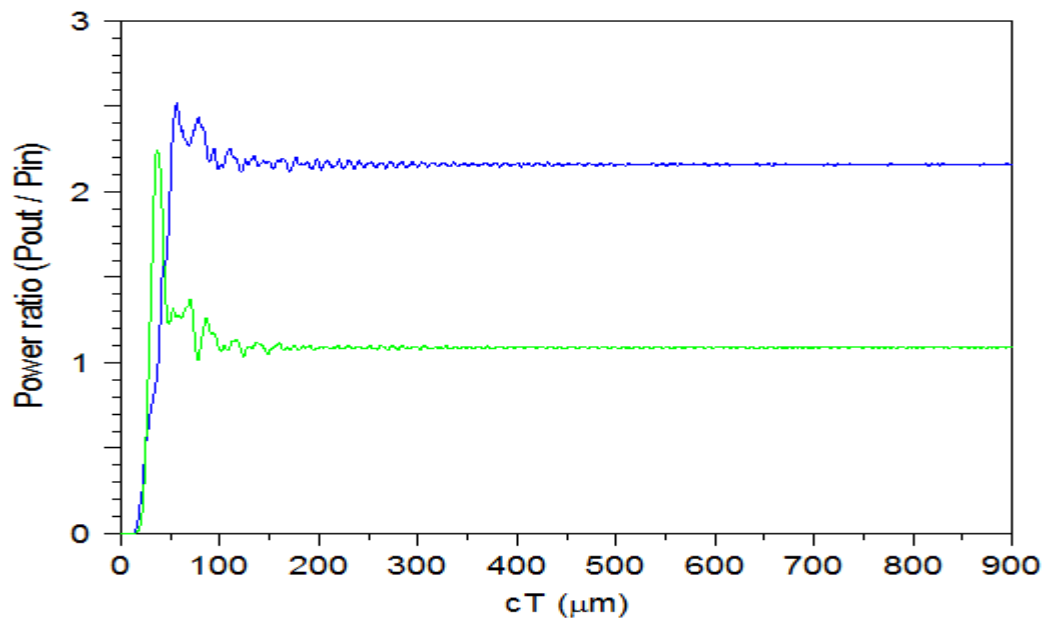


Figure 6.14: OPL at the ports SUM and CARRY for the input combinations A = 1, B = 1, and C = 1 (blue – SUM, green – CARRY)

6.3 Response Time Calculation

Time evolving curve has been used to evaluate the response time of the power obtained at the output SUM and CARRY ports. The same has been plotted in Figure 6.3.1 and 6.3.2 respectively. From figure 6.3.1, this curve shows optical transmission output for logic '1' at the port SUM, with the help of this curve we can calculate time response for port SUM. The total time required by the implemented structure in order to reach the maximum output power, 0 to 90% of the output average power can be analyzed using Figure 6.3.1. The average value P_{avg} attained here is 0.1606ps ($cT=48.18\mu m$), the product of speed of light (c) and total time (T). The total time comprises of the transmission delay (t_1) that can be defined as the average time taken by the output to reach from 0-10% of its maximum value (P_{avg}) and the delay time to reach 90%, i.e. the time taken by the output to reach from 10% to 90% of P_{avg} value. In this work these two timings can be defined as the time taken to reach 0.1%, t_1 which evaluates to 0.067ps ($cT=18.22\mu m$) and the time t_2 required by the output to reach from 0.1% to 90%, this value evaluates to 0.0936ps ($cT=$). The falling time where the output falls from P_{avg} to $0.1P_{avg}$ is almost equal to t_2 as the proposed structure here is dedicated for operation on linear material. The effective pulse width hence can be evaluated as $2t_2=0.1872ps$. When an output of 50% duty cycle is taken into consideration, the response time evaluates to 0.3744ps. From figure 6.3.2, this curve shows optical transmission output for logic '1' at the port CARRY, with the help of this curve we can calculate time response for port CARRY.

The total time required by the implemented structure in order to reach the maximum output power, 0 to 90% of the output average power can be analyzed using Figure 6.3.1. The average value P_{avg} attained here is 0.1247ps ($cT=24.2\mu m$), the product of speed of light (c) and total time (T). The total time comprises of the transmission delay (t_1) that can be defined as the average time taken by the output to reach from 0-10% of its maximum value (P_{avg}) and the delay time to reach 90%, i.e. the time taken by the output to reach from 10% to 90% of P_{avg} value. In this work these two timings can be defined as the time taken to reach 0.1%, t_1 which evaluates to 0.074ps ($cT=22.4\mu m$) and the time t_2 required by the output to reach from 0.1% to 90%, this value evaluates to 0.0507ps ($cT=\mu m$). The falling time where the output falls from P_{avg} to $0.1P_{avg}$ is almost equal to t_2 as the proposed structure here is dedicated for

operation on linear material. The effective pulse width hence can be evaluated as $2t_2=0.1014\text{ps}$. When an output of 50% duty cycle is taken into consideration, the response time evaluates to 0.2028ps . The CR of proposed FA is almost constant till 1550 nm of C-band (1530 nm to 1565 nm) to low reflection in either the unemployed input ports (less than 0.25 Pa). Reflection into unemployed input port gets almost improved to 0.45 Pa since 1550 nm wavelength is being considered. Therefore, a CR of a SUM output gets improved using the proposed design. Furthermore, the suggested structure ensures low reflection continuously in the C-band up to wavelengths of 1550 nm.

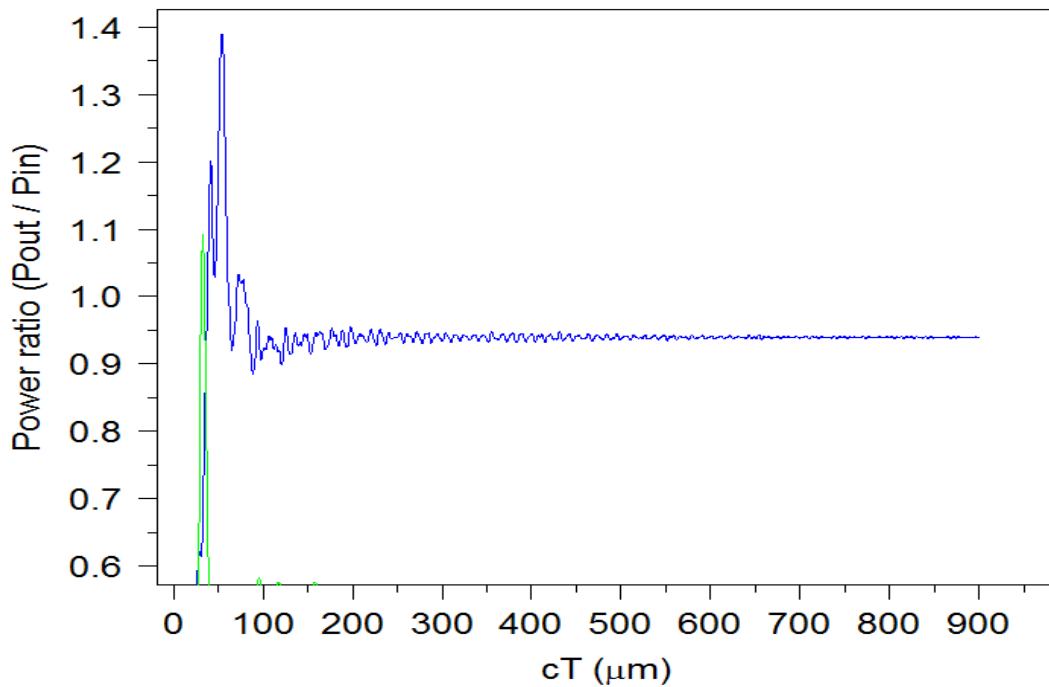


Figure 6.15: Time evolving curve from port SUM

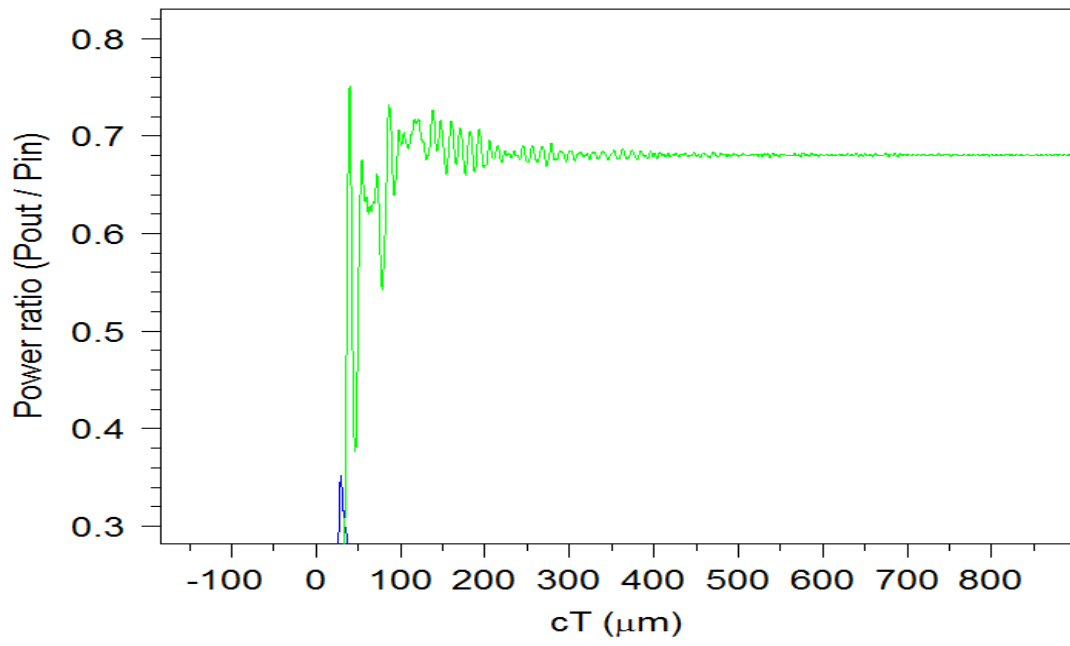


Figure 6.16: Time evolving curve from port CARRY

CHAPTER 7

CONCLUSION AND FUTURE SCOPE

7.1 Conclusions

I have proposed full adder structure using photonic crystal of three T- shaped. Three inputs and two outputs as the sum and carry an extra input introduced controlling input (Di). This additional input creates a phase between inputs based on interference. The contrast ratio of sum and carry is 12.5dB and 6.5 dB respectively. The fast response time of the proposed structure is 0.37ps. Also, the suggested structure works continuously with low reflection throughout the C-band up for 1550 nm.

7.2 Future scope

I have obtained CR for port SUM and CARRY is 12.5 and 6.5 respectively in this dissertation. The contrast ratios obtained shows the efficient performance of the implemented full adder however there still exists room for improvement. The efficiency of the designed full adder circuit can further be enhanced through effective optimizations. The reflections involved and power consumed can further be reduced which becomes necessary in real time applications. The application of the implemented system can be extended to combinational circuits such as multiplexers, decoders, encoders, subtractor etc.

REFERENCES

- [1] Yang, Yi-Pin, Kuen-Cherng Lin, I-Chen Yang, Kun-Yi Lee, Yen-Juei Lin, Wei-Yu Lee, and Yao-Tsung Tsai. "All-optical photonic crystal AND gate with multiple operating wavelengths." *Optics Communications* 297 (2013): 165-168.
- [2] Rani, Preeti, Yogita Kalra, and R. K. Sinha. "Realization of AND gate in Y shaped photonic crystal waveguide." *Optics Communications* 298 (2013): 227-231.
- [3] Rani, Preeti, Shiba Fatima, Yogita Kalra, and R. K. Sinha. "Realization of all optical logic gates using universal NAND gates on photonic crystal platform." *Superlattices and Microstructures* 109 (2017): 619-625.
- [4] Shaik, Enaul Haq, and Nakkeeran Rangaswamy. "Design of all-optical photonic crystal half adder with T-shaped waveguides using path difference based interference." In *2017 Progress in Electromagnetics Research Symposium-Fall (PIERS-FALL)*, pp. 2596-2602. IEEE, 2017.
- [5] Shaik, Enaul Haq, and Nakkeeran Rangaswamy. "Implementation of photonic crystal based all-optical half adder using T-shaped waveguides." In *2017 2nd International Conference on Computing and Communications Technologies (ICCCT)*, pp. 148-150. IEEE, 2017.
- [6] Alipour-Banaei, Hamed, and Hamed Seif-Dargahi. "Photonic crystal based 1-bit full-adder optical circuit by using ring resonators in a nonlinear structure." *Photonics and Nanostructures-Fundamentals and Applications* 24 (2017): 29-34.
- [7] Tang, Chunrong, Xinyu Dou, Yuxi Lin, Hongxi Yin, Bin Wu, and Qingchun Zhao. "Design of all-optical logic gates avoiding external phase shifters in a two-dimensional photonic crystal based on multi-mode interference for BPSK signals." *optics Communications* 316 (2014): 49-55.
- [8] Yang, Yi-Pin, Kuen-Cherng Lin, I-Chen Yang, Kun-Yi Lee, Yen-Juei Lin, Wei-Yu Lee, and Yao-Tsung Tsai. "All-optical photonic crystal AND gate with multiple operating wavelengths." *Optics Communications* 297 (2013): 165-168.

- [9] Jiang, Yu-Chi, Shao-Bin Liu, Hai-Feng Zhang, and Xiang-Kun Kong. "Reconfigurable design of logic gates based on a two-dimensional photonic crystal waveguide structure." *Optics communications* 332 (2014): 359-365.
- [10] Xavier, Susan C., and Kabilan P. Arunachalam. "Compact design of all-optical logic gates based on self-collimation phenomenon in two-dimensional photonic crystal" *Optical Engineering* 51, no. 4 (2012): 045201.
- [11] Rayleigh, Lord. "XXVI. On the remarkable phenomenon of crystalline reflexion described by Prof. Stokes." *The London, Edinburgh, and Dublin Philosophical Magazine and Journal of Science* 26, no. 160 (1888): 256-265.
- [12] Bykov, Vladimir P. "Spontaneous emission in a periodic structure." *Soviet Journal of Experimental and Theoretical Physics* 35 (1972): 269.
- [13] Bykov, Vladimir P. "Spontaneous emission from a medium with a band spectrum." *Soviet Journal of Quantum Electronics* 4, no. 7 (1975): 861.
- [14] Ohtaka, Kazuo. "Energy band of photons and low-energy photon diffraction." *Physical Review B* 19, no. 10 (1979): 5057.
- [15] John, Sajeev. "Strong localization of photons in certain disordered dielectric superlattices." *Physical review letters* 58, no. 23 (1987): 2486.
- [16] Li, Ying, Yuanjiang Xiang, Shuangchun Wen, Junhai Yong, and Dianyuan Fan. "Tunable terahertz-mirror and multi-channel terahertz-filter based on one-dimensional photonic crystals containing semiconductors." *Journal of Applied physics* 110, no. 7 (2011): 073111.
- [17] Weng, Libo. "An introduction to photonic crystals." *LC Optics and Photonics Course, Kent State University* (2012).
- [18] Yablonovitch, Eli, T. J. Gmitter, and Kok-Ming Leung. "Photonic band structure: The face-centered-cubic case employing nonspherical atoms." *Physical review letters* 67, no. 17 (1991): 2295.
- [19] Krauss, Thomas F., M. Richard, and Stuart Brand. "Two-dimensional photonic-bandgap structures operating at near-infrared wavelengths." *Nature* 383, no. 6602 (1996): 699.
- [20] Ouellette, Jennifer. "Seeing the future in photonic crystals." *The Industrial Physicist* 7, no. 6 (2001): 14-17.
- [21] Galusha, Jeremy W., Lauren R. Richey, John S. Gardner, Jennifer N. Cha, and Michael H. Bartl. "Discovery of a diamond-based photonic crystal structure in beetle scales." *Physical Review E* 77, no. 5 (2008): 050904.
- [22] Prasad, Paras N. *Nanophotonics*. John Wiley & Sons, 2004.
- [23] John, S. G. J., D. Joannopoulos, Joshua N. Winn, and Robert D. Meade. "Photonic crystals: molding the flow of light." In *Princeton University of press*. 2008.

- [24] Gaponenko, Sergey V. *Introduction to nanophotonics*. Cambridge University Press, 2010.
- [25] Maldovan, M., A. M. Urbas, N. Yufa, W. C. Carter, and E. L. Thomas. "Photonic properties of bicontinuous cubic microphases." *Physical Review B* 65, no. 16 (2002): 165123.
- [26] Ho, K. M., Che Ting Chan, and Costas M. Soukoulis. "Existence of a photonic gap in periodic dielectric structures." *Physical Review Letters* 65, no. 25 (1990): 3152.
- [27] Ho, Kin Ming, C. T. Chan, C. M. Soukoulis, R. Biswas, and M. Sigalas. "Photonic band gaps in three dimensions: new layer-by-layer periodic structures." *Solid State Communications* 89, no. 5 (1994): 413-416.
- [28] Joannopoulos, John D. "Photonics: Self-assembly lights up." *Nature* 414, no. 6861 (2001): 257.
- [29] Joannopoulos, John D., Steven G. Johnson, Joshua N. Winn, and Robert D. Meade. "Molding the flow of light." *Princeton Univ. Press, Princeton, NJ [ua]* (2008).
- [30] Taflove, Allen, and Susan C. Hagness. *Computational electrodynamics: the finite-difference time-domain method*. Artech house, 2005.
- [31] <https://www.physics-and-radio-electronics.com/physics/waveinterference.html>

Thesis

ORIGINALITY REPORT

15%

SIMILARITY INDEX

3%

INTERNET SOURCES

6%

PUBLICATIONS

7%

STUDENT PAPERS

PRIMARY SOURCES

1

Submitted to Indian School of Mines

Student Paper

5%

2

Enaul Haq Shaik, Nakkeeran Rangaswamy. "Design of all-optical photonic crystal half adder with T-shaped waveguides using path difference based interference", 2017 Progress in Electromagnetics Research Symposium - Fall (PIERS - FALL), 2017

Publication

3%

3

www.cadfamily.com

Internet Source

3%

4

Submitted to Higher Education Commission
Pakistan

Student Paper

1%

5

Preeti Rani, Shiba Fatima, Yogita Kalra, R.K. Sinha. "Realization of all optical logic gates using universal NAND gates on photonic crystal platform", Superlattices and Microstructures, 2017

Publication

1%
